JCB Journal of Cell Biology

ARTICLE

IRE1–XBP1 pathway regulates oxidative proinsulin folding in pancreatic β cells

Yuichi Tsuchiya[1*], Michiko Saito[1,2*], Hiroshi Kadokura[1,3], Jun-ichi Miyazaki[4], Fumi Tashiro[4], Yusuke Imagawa[1,5], Takao Iwawaki[6], and Kenji Kohno[1]

In mammalian pancreatic β cells, the IRE1α–XBP1 pathway is constitutively and highly activated under physiological conditions. To elucidate the precise role of this pathway, we constructed β cell–specific *Ire1a* conditional knockout (CKO) mice and established insulinoma cell lines in which *Ire1a* was deleted using the Cre–loxP system. *Ire1a* CKO mice showed the typical diabetic phenotype including impaired glycemic control and defects in insulin biosynthesis postnatally at 4–20 weeks. *Ire1a* deletion in pancreatic β cells in mice and insulinoma cells resulted in decreased insulin secretion, decreased insulin and proinsulin contents in cells, and decreased oxidative folding of proinsulin along with decreased expression of five protein disulfide isomerases (PDIs): PDI, PDIR, P5, ERp44, and ERp46. Reconstitution of the IRE1α–XBP1 pathway restored the proinsulin and insulin contents, insulin secretion, and expression of the five PDIs, indicating that IRE1α functions as a key regulator of the induction of catalysts for the oxidative folding of proinsulin in pancreatic β cells.

Introduction

ER stress and the unfolded protein response (UPR) have important implications for cellular functions and are linked to various human diseases including diabetes; accordingly, a detailed knowledge of these processes is critical. In metazoans, three principal ER stress sensors activate the UPR, i.e., PKR-like ER kinase (PERK), activating transcription factor 6 (ATF6), and inositol requiring 1 (IRE1; Rutkowski and Hegde, 2010; Kimata and Kohno, 2011). Among them, IRE1 is the mostly highly conserved from yeast to humans (Mori, 2009). Mammalian genomes encode two IRE1 paralogs, IRE1α and IRE1β. Whereas IRE1β is specifically expressed in digestive tissues such as the intestine and stomach, IRE1α is ubiquitously expressed (Bertolotti et al., 2001; Tsuru et al., 2013). Upon ER stress, IRE1α forms a dimer/oligomer for the trans-autophosphorylation and activation of its RNase domain (Kimata et al., 2007; Li et al., 2010). The activated IRE1α RNase domain then cleaves the unspliced form of X-box–binding protein 1 (*XBP1u*) mRNA to initiate the splicing of *XBP1u* mRNA on the ER membrane, leading to formation of the spliced form of *XBP1* (*XBP1s*; Yoshida et al., 2001; Calfon et al., 2002; Yanagitani et al., 2011). This splicing reaction creates a translational frameshift to produce functional XBP1s and a transcriptional activator that up-regulates genes encoding ER-associated degradation machinery proteins, ER chaperones, lipid synthesis enzymes, glycosylation enzymes, and secretory machinery proteins (Yoshida et al., 2003; Ron and Walter, 2007).

Pancreatic β cells synthesize and secrete a large amount of insulin in response to high-blood glucose concentrations. Accumulating evidence suggests that insulin production causes physiological ER stress and the activation of the UPR in pancreatic β cells (Hassler et al., 2015; Sharma et al., 2015; Szabat et al., 2016). Because some mutations in *PERK* are related to Wolcott–Rallison syndrome, the role of PERK in pancreatic β cells is well characterized (Harding et al., 2001, 2012). However, the role of IRE1α in pancreatic β cells, especially in the biosynthesis of insulin, is not fully understood (Lipson et al., 2006; Han et al., 2009).

Insulin is secreted from pancreatic β cells by regulated exocytosis in high-blood glucose conditions, and it is synthesized as preproinsulin from *Ins* genes. Preproinsulin is targeted to the ER membrane and, upon translocation, is processed to proinsulin. Proinsulin is folded via three disulfide bonds into its native structure (Weiss, 2009). Disulfide bond formation in the ER is catalyzed by protein disulfide isomerase (PDI) family proteins.

[1]Graduate School of Biological Sciences and Institute for Research Initiatives, Nara Institute of Science and Technology, Ikoma, Japan; [2]Bio-science Research Center, Kyoto Pharmaceutical University, Kyoto, Japan; [3]Institute of Multidisciplinary Research for Advanced Materials, Tohoku University, Sendai, Japan; [4]Division of Stem Cell Regulation Research, Osaka University Graduate School of Medicine, Suita, Japan; [5]Department of Molecular and Cellular Biology, Research Center, Osaka International Cancer Institute, Osaka, Japan; [6]Division of Cell Medicine, Department of Life Science, Medical Research Institute, Kanazawa Medical University, Uchinada, Japan.

*Y. Tsuchiya and M. Saito contributed equally to this paper; Correspondence to Kenji Kohno: kkouno@bs.naist.jp.

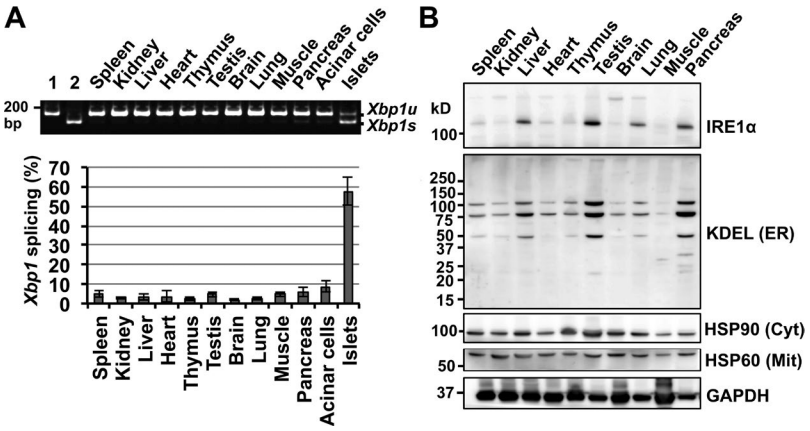

Figure 1. **Physiological activation of the IRE1α–XBP1 pathway in pancreatic islets. (A)** *Xbp1* mRNA splicing was analyzed by RT-PCR using total RNA isolated from the tissues of 8-wk-old WT male mice. The ratio of *Xbp1* mRNA splicing was quantified. Error bars show the means and SD. $n = 3$. *Xbp1* splicing (%) = *Xbp1s*/total *Xbp1* × 100. Lane 1, *Xbp1u*_pcDNA3.1(+). Lane 2, *Xbp1s*_pcDNA3.1(+). **(B)** Expression levels of IRE1α and ER-resident proteins harboring the KDEL motif (KDEL (ER)) in mouse tissues from an 8-wk-old WT male mouse based on immunoblotting. The expression levels of the cytosolic chaperone HSP90 (HSP90 (Cyt)) and the mitochondrial chaperone HSP60 (HSP60 (Mit)) were also examined. Positions of molecular mass markers are indicated on the left.

Mammals have at least 20 PDI family proteins (hereafter referred to as PDIs; Braakman and Bulleid, 2011; Okumura et al., 2015). The knockdown of PDI family genes results in decreased secretion of specific secretory proteins (Wang et al., 2007, 2015). However, it is not clear which PDI family proteins facilitate proinsulin folding.

To elucidate the physiological significance of the constitutive activation of the IRE1α–XBP1 pathway in pancreatic β cells, we established pancreatic β cell–specific *Ire1α* conditional knockout (CKO; IRE1α$^{B(-/\Delta R)}$) mice and insulinoma cells, MIN6 (*Ire1α*$^{fl/fl}$), harboring floxed *Ire1α* derived from *Ire1α*$^{fl/fl}$; IT-6 mice. Using these experimental models, we uncovered a new role of the IRE1α–XBP1 pathway in pancreatic β cells.

Results

Physiological activation of the IRE1α–XBP1 pathway in pancreatic β cells

Accumulating evidence suggests that the IRE1α–XBP1 pathway plays important roles in the pancreas at the neonatal and postnatal stages (Iwawaki et al., 2004; Lee et al., 2005, 2011). To directly observe the activation of the IRE1α–XBP1 pathway in adult mouse tissues, we used RT-PCR to examine the ratio of the spliced form of *Xbp1* mRNA to total *Xbp1* mRNA. In this analysis, *Xbp1* mRNA splicing was slightly higher in the pancreas than in other mouse tissues (Fig. 1 A). Consistent with the level of *Xbp1* mRNA splicing, both IRE1α and ER resident proteins harboring the KDEL motif (e.g., ER folding enzymes such as immunoglobulin heavy chain binding protein [BiP], GRP94, and PDI) exhibited higher expression in the pancreas of mice than chaperones localized in other cell compartments, including HSP90 in the cytosol and HSP60 in the mitochondria (Fig. 1 B).

The pancreas has two major types of secretory cells: exocrine acinar cells and endocrine islet cells. We observed moderate *Xbp1* mRNA splicing in pancreatic acinar cells but extremely high splicing in pancreatic islets (Fig. 1 A). β-Cells occupy ∼70% of pancreatic islets in mice (Pechhold et al., 2009) and humans (Wang et al., 2013). In addition, XBP1s protein is highly expressed in pancreatic islets in mice and humans (Engin et al., 2013, 2014). Collectively, these findings suggest that the IRE1α–XBP1 pathway is constitutively and highly activated under physiological conditions in pancreatic β cells in mammals.

Impaired glycemic control and defective insulin biosynthesis in IRE1α$^{B(-/\Delta R)}$ mice

To elucidate the role of the IRE1α–XBP1 pathway in pancreatic β cells, we generated pancreatic β cell–specific *Ire1α* CKO (IRE1α$^{B(-/\Delta R)}$) mice by crossing Ins-Cre mice (Herrera, 2000) with *Ire1α*$^{-/fl}$ mice (Iwawaki et al., 2009, 2010). The IRE1α$^{B(-/\Delta R)}$ mice exhibited steady increases in blood glucose beginning at 4 wk, whereas glucose levels in control (IRE1α$^{B(+/\Delta R)}$) mice did not increase (Fig. 2 A). In addition, the IRE1α$^{B(-/\Delta R)}$ mice showed more significant decreases in glucose tolerance than control IRE1α$^{B(+/\Delta R)}$ mice at 12 wk (Fig. 2 B). To understand the mechanism underlying the diabetic phenotype in IRE1α$^{B(-/\Delta R)}$ mice, we examined serum insulin levels. The IRE1α$^{B(-/\Delta R)}$ mice exhibited significantly lower serum insulin levels at 20 wk of age than IRE1α$^{B(+/\Delta R)}$ mice (Fig. 2 C). Consistent with this result, the intracellular contents of proinsulin and insulin were significantly decreased in the islets of IRE1α$^{B(-/\Delta R)}$ mice (Fig. 2, D and E), which explains the diabetic phenotype of IRE1α$^{B(-/\Delta R)}$ mice. However, the diabetic phenotype of IRE1α$^{B(-/\Delta R)}$ mice was not associated with changes in the size or number of pancreatic islets within 20 wk (Fig. S1, A–C). These findings indicate that IRE1α$^{B(-/\Delta R)}$ mice exhibited declined insulin secretion owing to a decreased capacity for insulin production and not a decreased number of islets or size of pancreatic β cells. Thus, these results suggest that the IRE1α–XBP1 pathway plays an important role in insulin production.

Establishment of a model cell line to study the role of IRE1α in pancreatic β cells

IRE1α$^{B(-/\Delta R)}$ mice showed a typical diabetic phenotype with hypoinsulinemia and hyperglycemia (Fig. 2). We examined the mechanism underlying defective insulin biosynthesis in IRE1α$^{B(-/\Delta R)}$ mice using a MIN6 cell line carrying a floxed *Ire1α*-RNase domain from a mouse obtained by crossing an IT-6 mouse expressing SV40 large T antigen under the control of the *INS* promoter (Miyazaki et al., 1990, 2010) with an *Ire1α*$^{fl/fl}$ mouse. This cell line was named MIN6 (*Ire1α*$^{fl/fl}$) (Fig. S2 A). We easily deleted the *Ire1α*-RNase domain from this model pancreatic β cell line by infecting the cells with adenovirus harboring Cre recombinase (Ad-Cre) referred to as Ad-Cre, MIN6 (*Ire1α*$^{\Delta R/\Delta R}$) (Fig. S2 B). After infection, cells were subjected to genotyping PCR and immunoblotting with an antibody against IRE1α. The results clearly showed that the IRE1α-RNase domain was almost completely deleted from MIN6

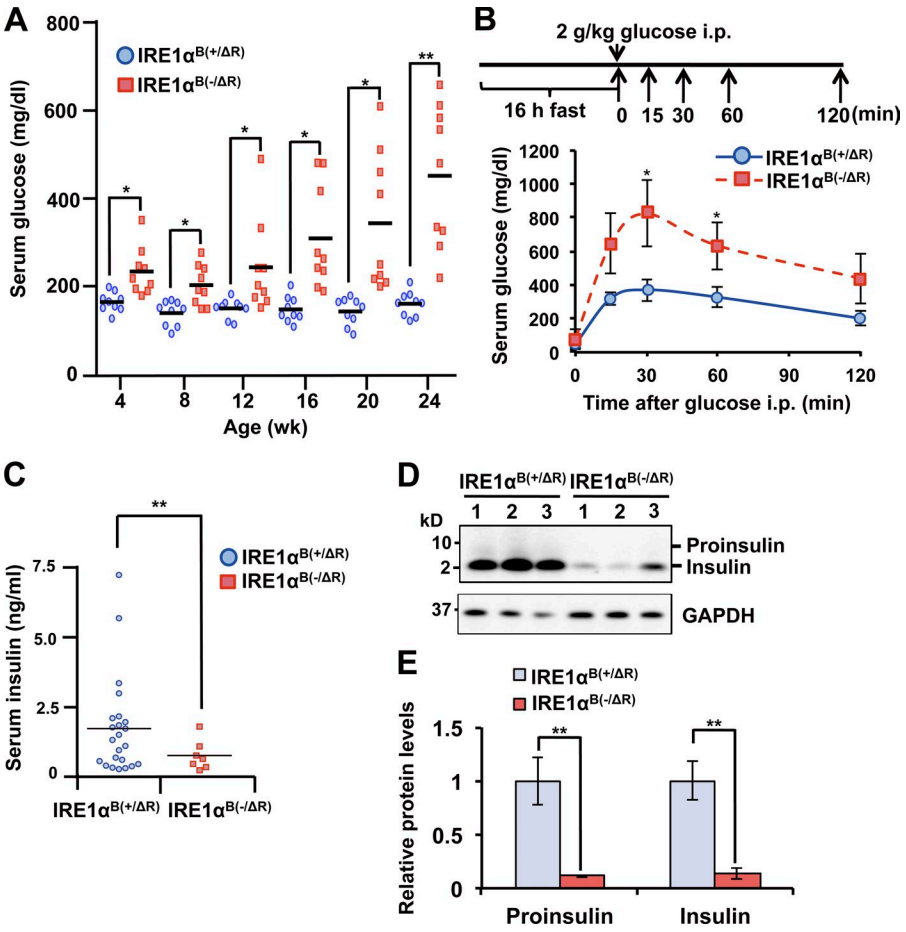

Figure 2. **Phenotypic analysis of pancreatic β cell–specific *Ire1α* CKO (IRE1α$^{B(-/\Delta R)}$) mice.** **(A)** Serum glucose in male mice of the indicated ages (wk). Horizontal lines show the means for each group; points show glucose measurements for individual mice in each group (IRE1α$^{B(+/\Delta R)}$ mice, blue points, n = 9; IRE1α$^{B(-/\Delta R)}$ mice, red points, n = 9). **(B)** Glucose tolerance of 12-wk-old male mice. Points show the means and SD for each group (IRE1α$^{B(+/\Delta R)}$ mice, n = 7; IRE1α$^{B(-/\Delta R)}$ mice, n = 5). Values for IRE1α$^{B(+/\Delta R)}$ and IRE1α$^{B(-/\Delta R)}$ mice are indicated by a blue solid line and a red dashed line, respectively. **(C)** Serum insulin levels of individual mice at 20 wk of age were measured by ELISA and are shown as points. The mean in each group is shown as a horizontal line (IRE1α$^{B(+/\Delta R)}$ mice, blue points, n = 23; IRE1α$^{B(-/\Delta R)}$ mice, red points, n = 7). **(D)** Detection of proinsulin and insulin in the pancreatic islets of male mice at 20 wk of age by immunoblotting. n = 3. **(E)** Protein expression levels of proinsulin and insulin relative to that of GAPDH in D were quantified and normalized by the value obtained for IRE1α$^{B(+/\Delta R)}$ mice. Blue bars indicate islets from IRE1α$^{B(+/\Delta R)}$ mice. Red bars indicate islets from IRE1α$^{B(-/\Delta R)}$ mice. Error bars show the means and SD for each group. n = 3. *, P < 0.05; **, P < 0.01 by Student's t test.

(*Ire1α*$^{fl/fl}$) cells after infection with Ad-Cre (Figs. 3 A and S2 C). Importantly, *Xbp1* mRNA splicing was completely inhibited in Ad-Cre, MIN6 (*Ire1α*$^{\Delta R/\Delta R}$) cells (Fig. 3, A and B).

Consistent with the results obtained for the islets of IRE1α$^{B(-/\Delta R)}$ mice, the intracellular contents of proinsulin and insulin in MIN6 (*Ire1α*$^{\Delta R/\Delta R}$) cells were remarkably decreased compared with those of control cells (Con, MIN6 (*Ire1α*$^{fl/fl}$) cells; adenovirus harboring GFP [Ad-GFP], MIN6 (*Ire1α*$^{fl/fl}$) cells; see Materials and methods; Fig. 3, A, C and D). Furthermore, insulin secretion from MIN6 (*Ire1α*$^{\Delta R/\Delta R}$) cells was dramatically decreased compared with that from MIN6 (*Ire1α*$^{fl/fl}$) cells (Fig. 3 E). Thus, MIN6 (*Ire1α*$^{\Delta R/\Delta R}$) cells retain the basic characteristics of the islets of IRE1α$^{B(-/\Delta R)}$ mice. Based on these findings, we used MIN6 (*Ire1α*$^{fl/fl}$) and MIN6 (*Ire1α*$^{\Delta R/\Delta R}$) cells as model cell lines to study the role of IRE1α in pancreatic β cells.

Morphology of insulin granules and the ER in MIN6 (*Ire1α*$^{\Delta R/\Delta R}$) cells

The insulin granule is the site of insulin maturation and storage before secretion from β cells. Because intracellular proinsulin and insulin contents were reduced in MIN6 (*Ire1α*$^{\Delta R/\Delta R}$) cells compared with control cells (Fig. 3, A, C, and D), we examined the number and size of insulin granules in MIN6 (*Ire1α*$^{\Delta R/\Delta R}$) cells by electron microscopy. The number of insulin granules was 27% lower in MIN6 (*Ire1α*$^{\Delta R/\Delta R}$) cells than in MIN6 (*Ire1α*$^{fl/fl}$) cells (Fig. 3, F–H). Furthermore, the size of insulin granules was significantly decreased in MIN6 (*Ire1α*$^{\Delta R/\Delta R}$) cells (Fig. 3, F, G, and I). These results are consistent with the decreased insulin content in MIN6 (*Ire1α*$^{\Delta R/\Delta R}$) cells.

Owing to their roles in ER homeostasis, deletion of ER stress sensors often results in abnormal ER morphology (Harding et al., 2001; Tsuru et al., 2013; Hassler et al., 2015). We examined the ER morphology in MIN6 (*Ire1α*$^{fl/fl}$) cells and observed a stacked sheetlike structure (Fig. 3 F, blue arrowheads). In contrast, the ER of MIN6 (*Ire1α*$^{\Delta R/\Delta R}$) cells showed a scattered small vesicle-like structure (Fig. 3 G, red arrowheads). These results indicate that the RNase activity of IRE1α is required for the maintenance of ER morphology in pancreatic β cells.

Activation of PERK and ATF6α in MIN6 (*Ire1α*$^{\Delta R/\Delta R}$) cells

The deletion of one of the three ER stress sensors in secretory cells often results in the activation of other ER stress sensors (Tsuru et al., 2013). Thus, we suspected that the deletion of IRE1α in pancreatic β cells might result in increased ER stress and activation of other ER stress sensors such as PERK and ATF6. To test this possibility, we examined whether PERK and ATF6 were more highly activated in MIN6 (*Ire1α*$^{\Delta R/\Delta R}$) cells. Upon ER stress, PERK phosphorylates PERK itself and eIF2α (Harding et al., 2001). Thus, to examine the activation of PERK, we quantified the phosphorylation of these proteins using antibodies that detect the phosphorylated forms. Levels of phosphorylated PERK and eIF2α were significantly higher in MIN6 (*Ire1α*$^{\Delta R/\Delta R}$) cells than in control cells (Fig. S3, A–C), indicating that PERK is more highly activated in MIN6 (*Ire1α*$^{\Delta R/\Delta R}$) cells. Mammals have

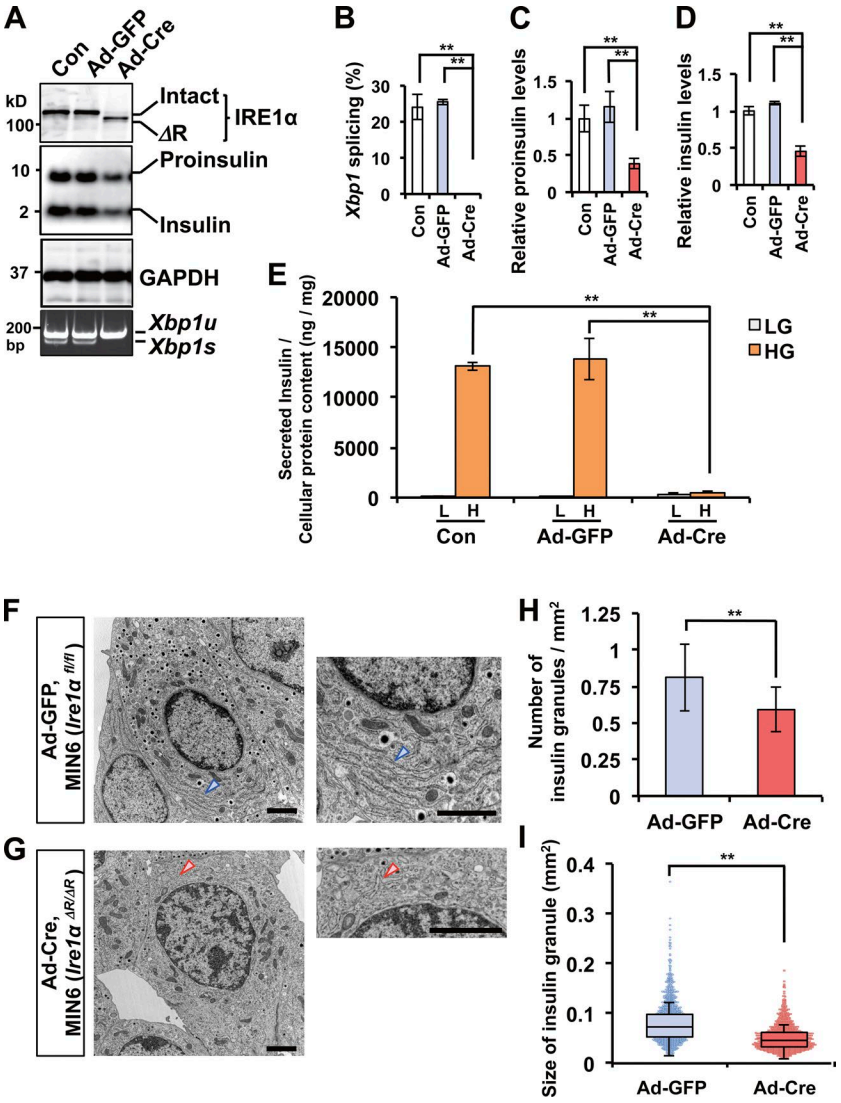

Figure 3. **Establishment of MIN6 cells lacking the IRE1α-RNase domain. (A–I)** MIN6 (*Ire1a*$^{fl/fl}$) cells were established and then infected with Ad-Cre to delete the RNase domain of *Ire1a*. MIN6 (*Ire1a*$^{fl/fl}$) cells infected with Ad-GFP were used as a control for adenovirus infection. Non–adenovirus-infected MIN6 (*Ire1a*$^{fl/fl}$) cells were also used as controls (Con). **(A)** Levels of IRE1α, proinsulin, insulin, and GAPDH were analyzed by immunoblotting in the indicated MIN6 cells. RT-PCR for *Xbp1* mRNA relative to total RNA isolated from the indicated MIN6 cells. **(B)** Splicing ratios of *Xbp1* mRNA in A were quantified. White bars indicate MIN6 (*Ire1a*$^{fl/fl}$) cells as a control (Con). Blue bars indicate MIN6 (*Ire1a*$^{fl/fl}$) cells infected with Ad-GFP. Red bars indicate MIN6 (*Ire1a*$^{\Delta R/\Delta R}$) cells infected with Ad-Cre. $n = 3$. **(C)** Protein expression levels of proinsulin relative to those of GAPDH in A were quantified and normalized by the value obtained for MIN6 (*Ire1a*$^{fl/fl}$) cells without adenovirus infection as a control (Con). Each bar presents the indicated MIN6 cells as described in B. **(D)** Protein expression levels of insulin relative to those of GAPDH in A were quantified and normalized as described in C. Each bar presents the indicated MIN6 cells as described in B. **(E)** Insulin secretion in response to various glucose concentrations in indicated MIN6 (*Ire1a*$^{fl/fl}$) cells was measured by ELISA. White bars indicate insulin secretion upon exposure to low glucose (LG). Orange bars indicate insulin secretion upon exposure to high glucose (HG). L indicates low glucose treatment (1.67 mM glucose/KRBH; 4 h). H indicates high glucose treatment (16.7 mM glucose/KRBH; 4 h). $n = 3$. **(F and G)** Sections of the indicated MIN6 cells were observed by transmission electron microscopy at 8,000×. **(F)** Sections of Ad-GFP, MIN6 (*Ire1a*$^{fl/fl}$) cells. The right panel is an enlarged part of the left panel. Blue arrowheads indicate the ER. **(G)** Sections of Ad-Cre, MIN6 (*Ire1a*$^{\Delta R/\Delta R}$) cells. The right panel is an enlarged part of the left panel. Red arrowheads indicate the ER. Bars, 2 µm. **(H)** Number of insulin granules per µm^2 in MIN6 (*Ire1a*$^{fl/f}$ or *Ire1a*$^{\Delta R/\Delta R}$) cells was quantified by using electron microscope images and calculated using ImageJ software. Error bars show means and SD. $n = 10$. **(I)** Sizes of insulin granules (µm^2) of MIN6 (*Ire1a*$^{fl/f}$ or *Ire1a*$^{\Delta R/\Delta R}$) cells were quantified as described in H. Results are summarized in box plots, and dots indicate individual size estimates of insulin granules. $n = 1{,}000$. **, $P < 0.01$.

two paralogs of *ATF6*: *ATF6α* and *ATF6β*. In response to ER stress, ATF6α and ATF6β are transported to the Golgi apparatus, where they are cleaved to release their cytosolic domain (Yamamoto et al., 2007). The level of cleaved ATF6α was slightly increased in MIN6 (*Ire1a*$^{\Delta R/\Delta R}$) cells (Fig. S3, D and E), indicating that ATF6α was slightly more activated in MIN6 (*Ire1a*$^{\Delta R/\Delta R}$) cells than in control cells. In contrast, the level of cleaved ATF6β was not significantly elevated in MIN6 (*Ire1a*$^{\Delta R/\Delta R}$) cells (Fig. S3, D and F). These results indicate that the deletion of the RNase domain of *Ire1a* causes the activation of PERK and ATF6α in MIN6 (*Ire1a*$^{\Delta R/\Delta R}$) cells. It has been reported that the constitutive activation of PERK and ATF6α causes CCAAT enhancer–binding protein (CHOP) induction (Arensdorf et al., 2013). *Chop* mRNA expression was slightly higher in MIN6 (*Ire1a*$^{\Delta R/\Delta R}$) cells than in control cells (Fig. S3 G). In pancreatic β cells, increased CHOP activity causes cell toxicity, e.g., sustained ER stress, oxidative stress, and apoptosis (Tabas and Ron, 2011). We examined whether the activation of PERK and ATF6α causes the decreased insulin secretion in MIN6 (*Ire1a*$^{\Delta R/\Delta R}$) cells. Treatment with a PERK kinase inhibitor, GSK 2606414 (Harding et al., 2012), and an ATF6α inhibitor, 4-(2-aminoethyl) benzylsulfonyl fluoride (AEBSF; Okada et al., 2003), did not restore insulin secretion in MIN6 (*Ire1a*$^{\Delta R/\Delta R}$) cells (Fig. S3 H). Thus, the activation of PERK and ATF6α is not the main factor explaining the decreased insulin secretion in MIN6 (*Ire1a*$^{\Delta R/\Delta R}$) cells.

Insulin mRNA levels are not altered in MIN6 (Ire1α$^{\Delta R/\Delta R}$) cells

The level of insulin secretion and cellular contents of proinsulin and insulin were substantially lower in Ad-Cre, MIN6 (*Ire1a*$^{\Delta R/\Delta R}$) cells than in control cells (Fig. 3, A and C–E). However, these decreases were not caused by activation of PERK and ATF6 (Fig. S3 H), suggesting that efficient insulin biosynthesis requires the IRE1α–XBP1 pathway. To understand the role of IRE1α in the biosynthesis of insulin, we first examined the effect of the deletion of the IRE1α-RNase domain on the transcription of *Ins* genes. Mice have two *Ins* paralogs: *Ins1* and *Ins2*. *Ins* genes are up-regulated

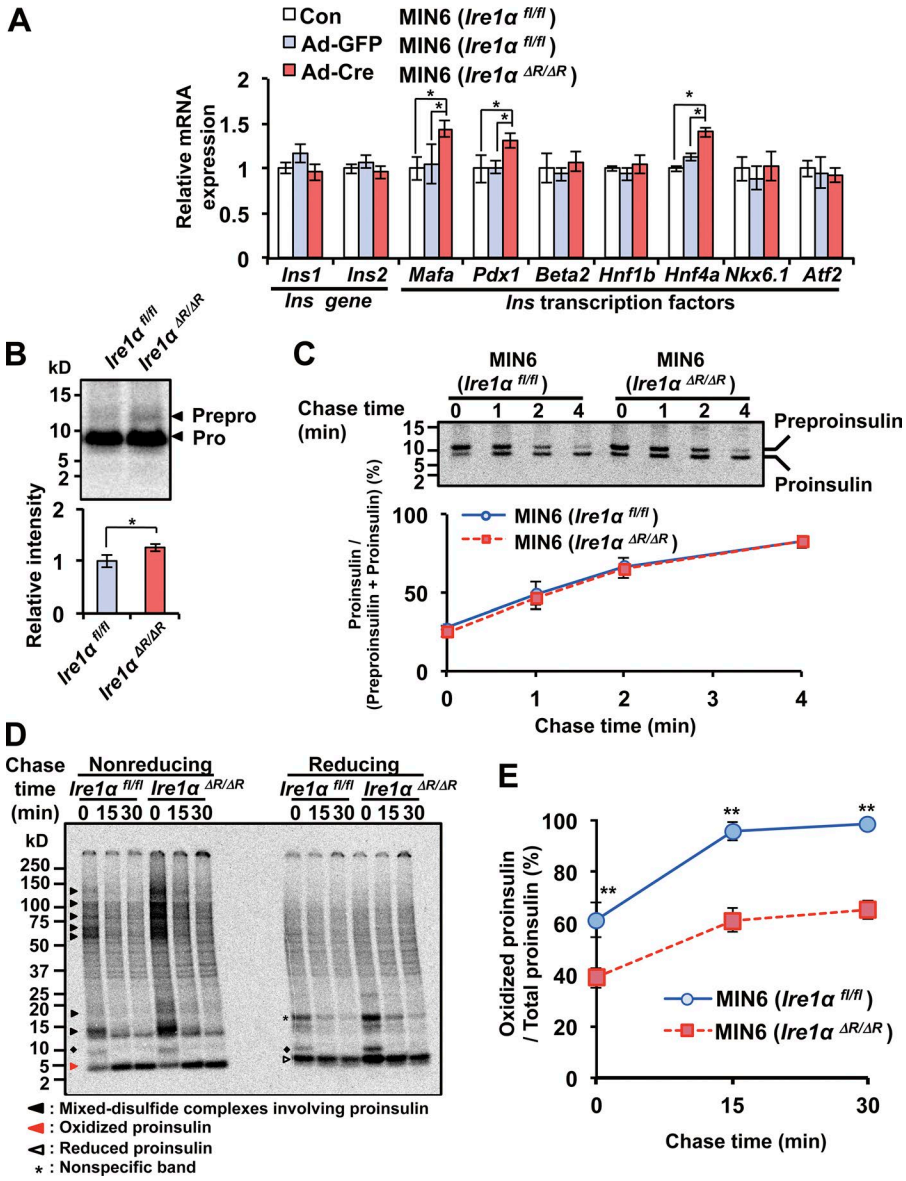

Figure 4. **Decreased oxidative folding of proinsulin in IRE1α-RNase domain KO MIN6 cells.** **(A)** Levels of *Ins* genes and transcription factors that regulate *Ins* genes relative to *Gapdh* expression levels in the indicated MIN6 cells were measured by qRT-PCR. White bars indicate control MIN6 (*Ire1a*$^{fl/fl}$) cells (Con). Blue bars indicate MIN6 (*Ire1a*$^{fl/fl}$) cells infected with Ad-GFP. Red bars indicate MIN6 (*Ire1a*$^{\Delta R/\Delta R}$) cells infected with Ad-Cre. **(B)** To detect newly synthesized preproinsulin and proinsulin in the indicated MIN6 cells, MIN6 cells were pulsed with [^{35}S]Met/Cys for 30 min. Radiolabeled preproinsulin and proinsulin were then immunoprecipitated, separated by NuPAGE, and detected by autoradiography. The ratio of the translation of preproinsulin and proinsulin in MIN6 (*Ire1a*$^{\Delta R/\Delta R}$) cells to that of MIN6 (*Ire1a*$^{fl/fl}$) cells was quantified. Blue bar, MIN6 (*Ire1a*$^{fl/fl}$) cells; red bar, MIN6 (*Ire1a*$^{\Delta R/\Delta R}$) cells. **(C)** To compare the rate of conversion from preproinsulin to proinsulin in MIN6 (*Ire1a*$^{fl/fl}$ or *Ire1a*$^{\Delta R/\Delta R}$) cells, the cells were pulsed for 1 min with [^{35}S] Met/Cys and then chased for the indicated times. The ratio of proinsulin to the sum of preproinsulin and proinsulin was quantified. The values for MIN6 (*Ire1a*$^{fl/fl}$) and MIN6 (*Ire1a*$^{\Delta R/\Delta R}$) cells are indicated by a blue solid line and by a red broken line, respectively. The values obtained did not differ significantly among time points by Student's *t* test. **(D)** To compare the rate of oxidative folding of proinsulin in MIN6 (*Ire1a*$^{fl/fl}$ or *Ire1a*$^{\Delta R/\Delta R}$) cells, the cells were pulsed for 5 min with [^{35}S]Met/Cys and then chased for the indicated times. Radiolabeled proinsulin was immunoprecipitated with an antiproinsulin antibody, boiled with (Reducing) or without (Nonreducing) DTT, separated by NuPAGE, and detected by autoradiography. The closed diamond indicates preproinsulin. **(E)** The ratio of oxidized proinsulin (left, red arrowhead) to total proinsulin (right, white arrowhead) in D was quantified. Error bars represent means and SD for each group. $n = 3$. *, $P < 0.05$; **, $P < 0.01$.

by various transcription factors such as Pdx1, MafA, and Beta2 (Han et al., 2011). To determine whether IRE1α is involved in *Ins* gene transcription in pancreatic β cells, we examined the effect of IRE1α-RNase deficiency on the expression levels of *Ins* genes and related transcription factors in MIN6 cells. The expression levels of *Ins1* and *Ins2* were not decreased in MIN6 (*Ire1a*$^{\Delta R/\Delta R}$) cells (Fig. 4 A). Moreover, the expression levels of genes encoding transcription factors that regulate *Ins* genes were not decreased in MIN6 (*Ire1a*$^{\Delta R/\Delta R}$) cells (Fig. 4 A). These findings indicate that the IRE1α–XBP1 pathway is not involved in the regulation of *Ins* gene transcription, at least under the tested conditions, in pancreatic β cells.

Translation and translocation of preproinsulin in MIN6 (*Ire1a*$^{\Delta R/\Delta R}$) cells

Next, we examined the role of the IRE1α–XBP1 pathway in the translation and translocation of insulin in pancreatic β cells. To examine the translation of *Ins* mRNA, MIN6 cells were labeled with [^{35}S]Met/Cys for 30 min and subjected to immunoprecipitation (Fig. 4 B). Preproinsulin and proinsulin levels did not differ between MIN6 (*Ire1a*$^{\Delta R/\Delta R}$) cells and MIN6 (*Ire1a*$^{fl/fl}$) cells (Fig. 4 B), indicating that the IRE1α–XBP1 pathway is not required for efficient translation of *Ins* mRNAs. To examine the translocation of preproinsulin into the ER, cells were pulse-labeled for 1 min, chased, and subjected to immunoprecipitation. During or immediately after translocation into the ER, the signal sequence of preproinsulin is processed to form proinsulin. As expected, the majority of preproinsulin was converted to proinsulin during the chase period. The processing rate of the signal sequence of preproinsulin did not differ between MIN6 (*Ire1a*$^{\Delta R/\Delta R}$) cells and MIN6 (*Ire1a*$^{fl/fl}$) cells (Fig. 4 C). Thus, the IRE1α–XBP1 pathway is not required for the efficient translocation of preproinsulin into the ER.

Detection of mixed-disulfide complexes involving proinsulin

The formation of disulfide bridges between the correct pairs of cysteines, which is presumably mediated by PDI family members, is vital for the folding of most secretory proteins with disulfide

bonds. PDI family members catalyze the formation, isomerization, and reduction of disulfide bonds. During the reactions, PDI family members form disulfide-linked intermediates with their substrates. Despite their transience, the intermediates can be stabilized by treating cells directly with TCA to prevent post-harvest oxidation of cysteines and then alkylating the free cysteines with *N*-ethylmaleimide (NEM). In this experiment, we combined this method with pulse-chase experiments and used a high-titer antibody against newly synthesized proinsulin to follow the oxidative folding of proinsulin (Kadokura and Beckwith, 2009; Kadokura et al., 2013). WT MIN6 cells (Miyazaki et al., 1990, 2010) were labeled with [^{35}S]Met/Cys for 5 min, chased for up to 60 min, and treated with TCA and subjected to immunoprecipitation with an antiproinsulin antibody. Immediately after the pulse, a small fraction of proinsulin was observed at the oxidized position (5.5 kD; Fig. S4 A, red arrowhead). In addition to this band, several bands with different molecular masses were observed from 15–250 kD (Fig. S4 A, black arrowheads). After a 15-min chase, appreciable portions of bands were converted to oxidized proinsulin (Fig. S4 A). To examine whether the bands observed from 15–250 kD indeed contained proinsulin, after pulse labeling, samples were analyzed by 2D gel electrophoresis in which the first dimension was nonreducing and the second was reducing. Appreciable portions of the bands observed from 15–250 kD in the first dimension (Fig. S4 B, black arrowheads) were shifted to the position corresponding with the reduced form of proinsulin (9 kD) in the second dimension (Fig. S4 B, white arrowhead). These bands represented mixed-disulfide complexes involving proinsulin. Some nonspecific bands showed resistance to β-mercaptoethanol treatment.

Inefficient folding of proinsulin in MIN6 (*Ire1α*$^{\Delta R/\Delta R}$) cells

To study the role of IRE1α in the oxidative folding of proinsulin, we monitored the folding status of proinsulin in MIN6 (*Ire1α*$^{\Delta R/\Delta R}$) cells by calculating the ratio of oxidized proinsulin (Fig. 4 D, Nonreducing, red arrowhead) to total proinsulin (Fig. 4 D, Reducing, white arrowhead; and Fig. 4 E). In MIN6 (*Ire1α*$^{fl/fl}$) cells, the ratio of folded proinsulin to total proinsulin increased during the chase. Importantly, in MIN6 (*Ire1α*$^{\Delta R/\Delta R}$) cells, the ratio of folded proinsulin to total proinsulin was significantly lower than that of control MIN6 cells (Fig. 4 E). From these findings, we concluded that oxidative folding of proinsulin was significantly decreased in MIN6 (*Ire1α*$^{\Delta R/\Delta R}$) cells.

Expression levels of PDIs and ER chaperones in MIN6 (*Ire1α*$^{\Delta R/\Delta R}$) cells and islets of IRE1α$^{B(-/\Delta R)}$ mice

Oxidative folding of proinsulin takes place in the ER and is assisted by PDI family members and ER chaperones. However, the precise mechanisms of proinsulin folding, including the enzymes involved in this process, remain unclear. Because the oxidative folding of proinsulin was decreased in MIN6 (*Ire1α*$^{\Delta R/\Delta R}$) cells, we speculated that IRE1α up-regulates some ER chaperones and PDIs involved in proinsulin folding in pancreatic β cells. To identify such enzymes and chaperones, we compared the expression levels of ER chaperones and PDIs in MIN6 cells by quantitative real-time PCR (qRT-PCR; Fig. S4, C and D). Among PDI family proteins, the expression levels of *Pdi*, *Pdir*, *Pdip*, *P5*, *Erp44*, *Erp46*, and *Erdj5/Jpdi* were significantly lower in MIN6 (*Ire1α*$^{\Delta R/\Delta R}$) cells than in MIN6 (*Ire1α*$^{fl/fl}$) cells (Fig. S4 D). In contrast, among ER chaperones, decreased expression levels were observed only for *Erdj4* and *Orp150* (Fig. S4 C). We further examined the protein expression levels of ER chaperones and PDIs by immunoblotting. ORP150 expression was slightly lower in MIN6 (*Ire1α*$^{\Delta R/\Delta R}$) cells than in MIN6 (*Ire1α*$^{fl/fl}$) cells, and the levels of PDI/PDIA1, PDIR/PDIA5, P5/PDIA6, ERp44/PDIA10, and ERp46/PDIA15 were substantially lower in MIN6 (*Ire1α*$^{\Delta R/\Delta R}$) cells (Fig. 5, A and B). ERdj4 and PDIp/PDIA2 were not detectable by immunoblotting in either MIN6 (*Ire1α*$^{fl/fl}$) cells or MIN6 (*Ire1α*$^{\Delta R/\Delta R}$) cells (not depicted). Next, we examined the expression levels of the five PDIs and ORP150 in islets of IRE1α$^{B(-/\Delta R)}$ mice by immunoblotting. Consistent with the results in MIN6 (*Ire1α*$^{\Delta R/\Delta R}$) cells, the levels of PDI, PDIR, P5, ERp44, ERp46, and ORP150 were significantly and specifically lower in the pancreatic islets of IRE1α$^{B(-/\Delta R)}$ mice than in those of IRE1α$^{B(+/\Delta R)}$ mice (Fig. 5, C and D). From these findings, we concluded that the IRE1α–XBP1 pathway is required for efficient induction of PDI, PDIR, P5, ERp44, ERp46, and ORP150.

Insulin secretion and insulin content were restored by reconstitution of the IRE1α–XBP1 pathway in MIN6 (*Ire1α*$^{\Delta R/\Delta R}$) cells

To examine whether insulin secretion and insulin content could be restored by reconstituting the IRE1α–XBP1 pathway in MIN6 (*Ire1α*$^{\Delta R/\Delta R}$) cells, we stably expressed WT *Ire1α* or *Xbp1s* in the mutant MIN6 cells. As expected, the splicing of XBP1 was restored by the expression of WT *Ire1α* or *Xbp1s* in MIN6 (*Ire1α*$^{\Delta R/\Delta R}$) cells (Fig. 6, A and B). Importantly, the stable expression of one of these genes also fully restored the intracellular contents of proinsulin and insulin (Fig. 6, A, C, and D) and moderately restored insulin secretion in high-glucose conditions (Fig. 6 E) in MIN6 (*Ire1α*$^{\Delta R/\Delta R}$) cells. Moreover, the expression levels of the five PDIs, i.e., PDI, PDIR, P5, ERp44, and ERp46, were also restored in MIN6 (*Ire1α*$^{\Delta R/\Delta R}$) cells stably expressing WT *Ire1α* or *Xbp1s* (Fig. 6, F and G). These findings clearly support the idea that the IRE1α–XBP1 pathway is responsible for the oxidative folding of proinsulin and the elevated expression of the five PDIs in pancreatic β cells.

XBP1s directly binds to the promoter regions of the five PDI family genes

XBP1s binds to the ACGT core sequence of the UPR element in the promoter regions of downstream target genes such as *Hspa5* (BiP; Acosta-Alvear et al., 2007). The five PDI family genes also have ACGT core sequences in their promoter regions. To examine whether XBP1s directly binds to the promoter regions of the five PDI family genes, we performed a chromatin immunoprecipitation (chIP) assay using a nuclear extract from WT MIN6 cells. The PCR amplification of the chIP revealed that XBP1s directly binds to the promoter regions of the five PDI family genes (Fig. 7).

Detection of covalent interactions between PDIs and proinsulin

Based on the decreased expression of the five PDIs in MIN6 (*Ire1α*$^{\Delta R/\Delta R}$) cells and pancreatic islets of IRE1α$^{B(-/\Delta R)}$ mice, we speculated that some are involved in the proinsulin folding process. During oxidative folding, PDI family members form

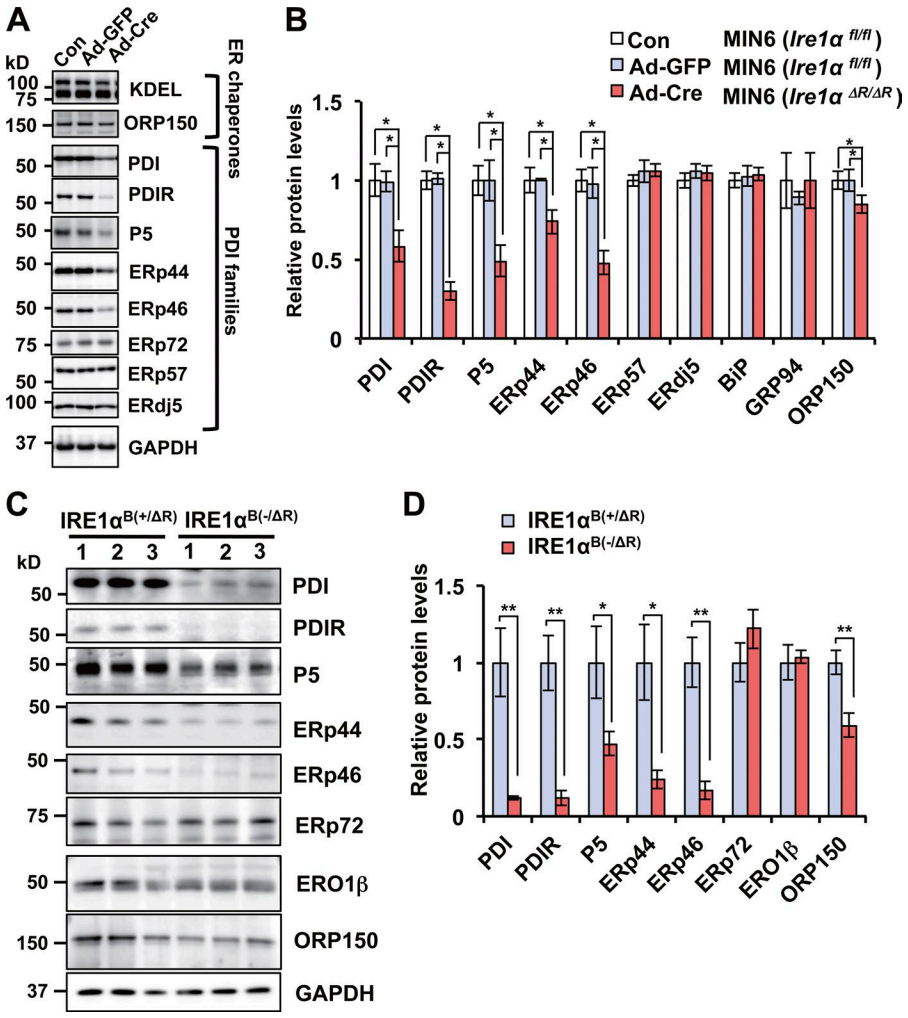

Figure 5. **Expression levels of ER chaperones and PDI family proteins in MIN6 (*Ire1α*$^{\Delta R/\Delta R}$) cells and pancreatic islets of IRE1α$^{B(-/\Delta R)}$ mice.** **(A)** Expression levels of PDI family proteins and ER chaperones in the MIN6 (*Ire1α*$^{fl/fl}$ or *Ire1α*$^{\Delta R/\Delta R}$) cells were analyzed by immunoblotting. **(B)** Expression levels of PDI family proteins and ER chaperones relative to the GAPDH expression in the MIN6 (*Ire1α*$^{fl/fl}$ or *Ire1α*$^{\Delta R/\Delta R}$) cells in A were measured by immunoblotting and normalized by the value obtained for MIN6 (*Ire1α*$^{fl/fl}$) cells without adenovirus infection (Con). White bars indicate control MIN6 (*Ire1α*$^{fl/fl}$) cells (Con). Blue bars indicate MIN6 (*Ire1α*$^{fl/fl}$) cells infected with Ad-GFP. Red bars indicate MIN6 (*Ire1α*$^{\Delta R/\Delta R}$) cells infected with Ad-Cre. **(C)** Expression levels of PDI family proteins and ER chaperones in pancreatic islets from the indicated mice at 24 wk of age were analyzed by immunoblotting. **(D)** Expression levels of PDI family proteins and ER chaperones relative to those of GAPDH in C were quantified and normalized by the value of control mice. Blue bars indicate islets from IRE1α$^{B(+/\Delta R)}$ mice. Red bars indicate islets from IRE1α$^{B(-/\Delta R)}$ mice. Error bars show means and SD for each group. $n = 3$. *, $P < 0.05$; **, $P < 0.01$.

transient disulfide-linked intermediates with their substrates (Kadokura et al., 2013). To test whether it is possible to detect covalent interactions between PDI family members and proinsulin, MIN6 cells were transfected with FLAG-tagged PDI, P5, ERp44, ERp46, and ERp72 (Araki et al., 2013). We detected specific bands with greater molecular masses than that of monomer proinsulin by nonreducing electrophoresis (Figs. 8 A and S4, A and B, black arrowheads). These bands represent disulfide-linked complexes formed between proinsulin and one of the PDI family members (PDI, P5, ERp44, or ERp46) as indicated by their conversion to the reduced form of monomer proinsulin after treatment with a reductant before electrophoresis (Fig. 8 A, white arrowhead). These findings indicate that PDI, P5, ERp44, ERp46, and ERp72 indeed interact with proinsulin via a disulfide bond at some point during the biosynthesis of proinsulin. Among the PDI family proteins tested in this experiment, PDI, P5, ERp44, and ERp46, which are downstream targets of the IRE1α–XBP1 pathway, are involved in disulfide formation of proinsulin. Compared with PDI, P5, ERp44, and ERp46, PDIR had relatively minor contribution to disulfide formation of proinsulin, at least in this experiment (Fig. 8 A). Next, we examined whether reconstitution of the five PDIs, i.e., PDI, PDIR, P5, ERp44, and ERp46, can restore insulin secretion in MIN6 (*Ire1α*$^{\Delta R/\Delta R}$) cells. In this experiment, we used Cys-dead (CM) PDI mutants (CM PDIs) as a negative control. When we transiently expressed the WT five PDIs in MIN6 (*Ire1α*$^{\Delta R/\Delta R}$) cells as shown in Fig. 8 B, insulin secretion was restored to a similar extent (~50% compared with MIN6 (*Ire1α*$^{fl/fl}$)) as the results obtained by the reconstitution of *Ire1α* in MIN6 (*Ire1α*$^{\Delta R/\Delta R}$) cells (~55% compared with MIN6 (*Ire1α*$^{fl/fl}$) cells in Fig. 6 E). It is important to note that overexpression of the WT five PDIs in MIN6 (*Ire1α*$^{fl/fl}$) cells resulted in a 17% increase in insulin secretion, whereas overexpression of the only PDI/PDIA1 in MIN6 (*Ire1α*$^{fl/fl}$) cells revealed a 13% decrease (Fig. 8 C). This result strongly supports our idea that the five PDIs participate in the proinsulin folding process in the ER.

Discussion

In this study, we presented several lines of evidence that the IRE1α–XBP1 pathway plays an important role in the efficient folding of proinsulin and transcriptional induction of the five PDI family proteins, which are critical for correct disulfide bond formation of proinsulin, in pancreatic β cells. We tried to detect both oxidized monomer proinsulin and mixed-disulfide complexes between proinsulin and PDI family proteins to monitor the accurate speed of oxidative folding of proinsulin by an improved method of pulse-chase experiments (see Materials and methods;

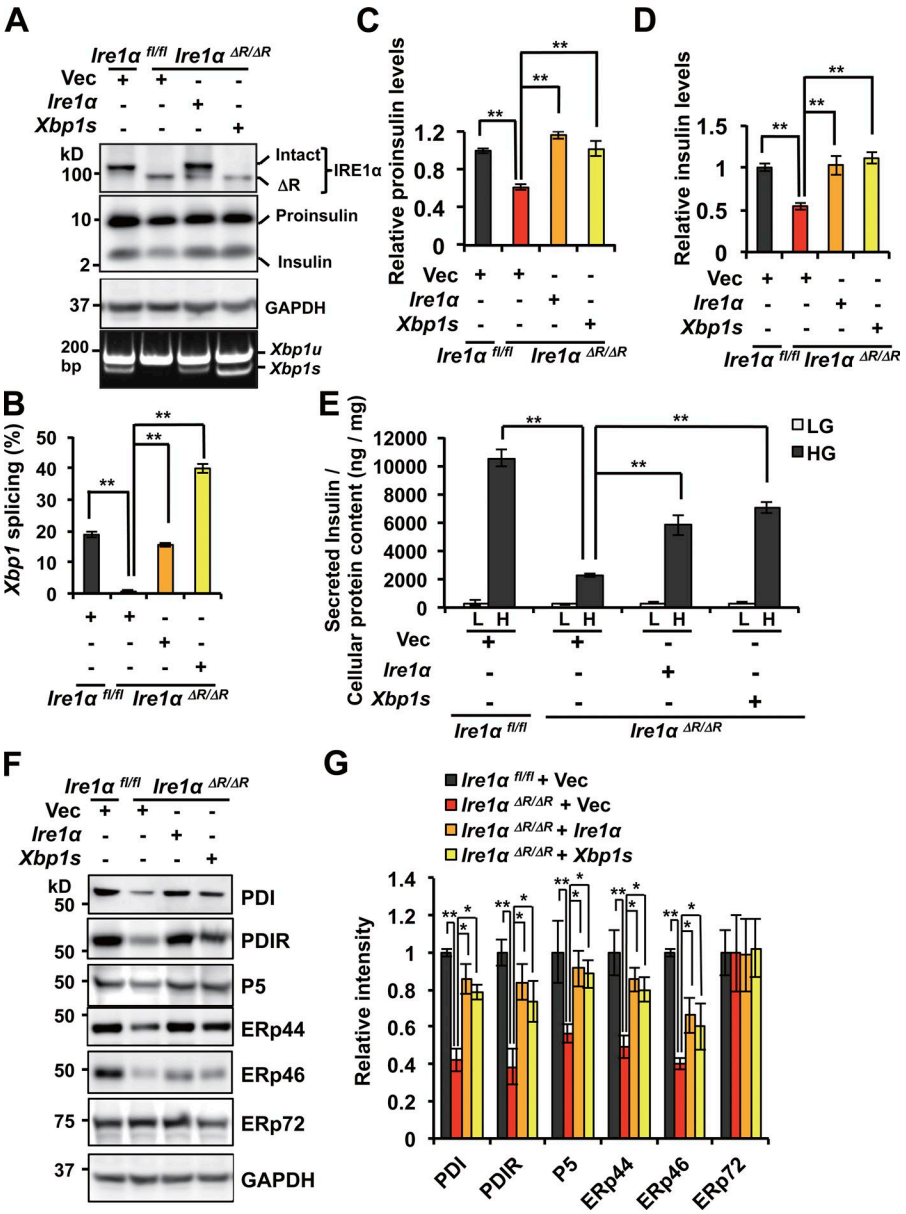

Figure 6. **Reconstitution of the IRE1α–XBP1 pathway in MIN6 (*Ire1α*$^{ΔR/ΔR}$) cells. (A–G)** To examine whether the phenotype of MIN6 (*Ire1α*$^{ΔR/ΔR}$) cells is restored by reconstituting the IRE1α–XBP1 pathway, WT *Ire1α* and *Xbp1s* were stably expressed by retroviruses harboring WT *Ire1α* and *Xbp1s* in MIN6 (*Ire1α*$^{ΔR/ΔR}$) cells, respectively. In B, C, D, and G, black bars indicate MIN6 (*Ire1α*$^{fl/fl}$) cells infected with retrovirus harboring an empty vector (Vec). Red bars indicate MIN6 (*Ire1α*$^{ΔR/ΔR}$) cells infected with retrovirus harboring an empty vector. Orange bars indicate MIN6 (*Ire1α*$^{ΔR/ΔR}$) cells infected with retrovirus harboring WT *Ire1α*. Yellow bars indicate MIN6 (*Ire1α*$^{ΔR/ΔR}$) cells infected with retrovirus harboring *Xbp1s*. **(A)** Expression levels of IRE1α, proinsulin, insulin, and GAPDH were analyzed by immunoblotting in the indicated MIN6 cells. RT-PCR for *Xbp1* mRNA of total RNA isolated from the indicated MIN6 cells. **(B)** The ratio of *Xbp1* mRNA splicing in A was quantified. *Xbp1* splicing (%) = *Xbp1s*/total *Xbp1* × 100. **(C)** Expression levels of proinsulin relative to the GAPDH expression in A were quantified and normalized by the value obtained for MIN6 (*Ire1α*$^{fl/fl}$) cells infected with retrovirus harboring an empty vector. **(D)** Expression levels of insulin relative to those of GAPDH in A were quantified and normalized as described in C. **(E)** Insulin secretion in response to glucose concentration in the indicated MIN6 cells for 4 h was measured by ELISA. White and black bars indicate insulin secretion upon exposure to low (L; 1.67 mM glucose/KRBH; 4 h) and high (H; 16.7 mM glucose/KRBH; 4 h) glucose, respectively. HG, high glucose; LG, low glucose. **(F)** Expression levels of PDI family proteins and ER chaperones in the indicated MIN6 cells were analyzed by immunoblotting. **(G)** Protein expression levels of PDI family proteins and ER chaperones relative to those of GAPDH in F were quantified and normalized as described in C. Error bars represent means and SD. *n* = 3. *, P < 0.05; **, P < 0.01.

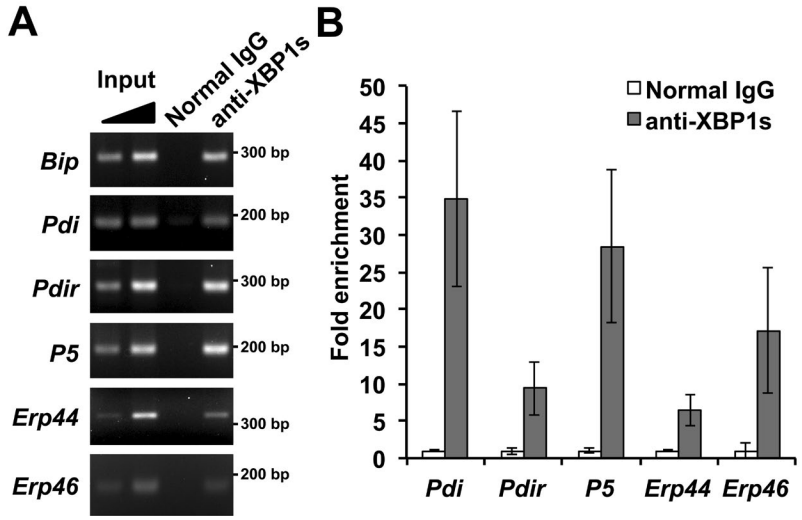

Figure 7. **XBP1s directly binds to the promoter regions of the five PDI family genes. (A)** ChIP assay using normal IgG and anti–XBP1s IgG. PCR of the WT MIN6 cell extracts were performed using a set of primers outside of the promoter regions containing XBP1s binding sites. **(B)** ChIP assay followed by quantitative PCR to quantify the binding of XBP1s to proximal promoter regions of the indicated genes. Error bars indicate means and SD. *n* = 3.

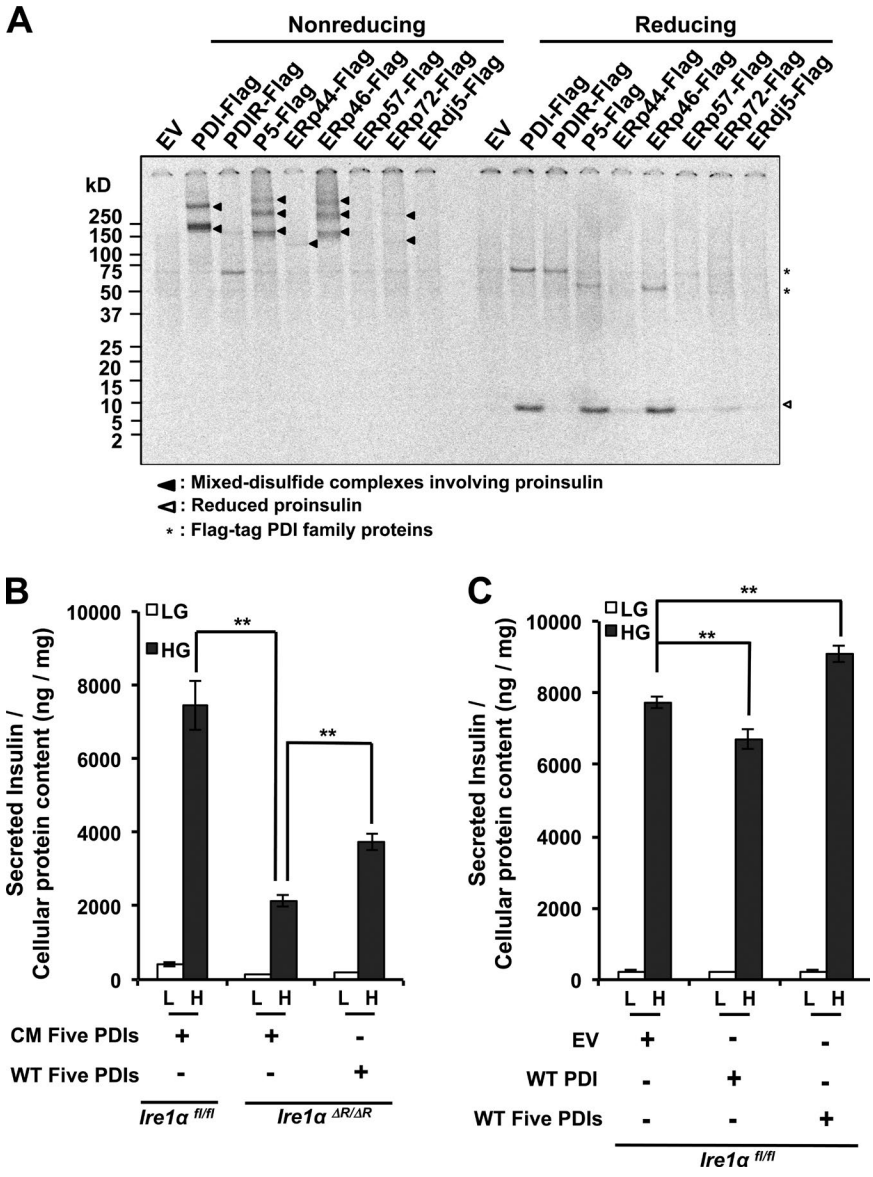

Figure 8. **Detection of mixed-disulfide complexes between proinsulin and PDI family members in MIN6 cells and reconstitution of the five PDIs in MIN6 (*Ire1α*$^{\Delta R/\Delta R}$) cells. (A)** Cys-mediated interaction between PDI family proteins and newly synthesized proinsulin during proinsulin folding. WT MIN6 cells were transiently transfected with indicated FLAG-tagged PDI family proteins, pulsed for 5 min with [^{35}S]Met/Cys, directly treated with TCA, and subjected to alkylation with NEM. Mixed-disulfide complexes between PDIs and proinsulin were collected by consecutive immunoprecipitation (first immunoprecipitation by anti-FLAG antibody; second immunoprecipitation by antiproinsulin antibody). After elution, samples were treated with (Reducing) or without (Nonreducing) DTT, separated by NuPAGE, and detected by autoradiography. **(B)** MIN6 (*Ire1α*$^{\Delta R/\Delta R}$) cells were transiently transfected with WT five PDIs or five CM PDIs. The expression of insulin was induced by culturing cells for 4 h in the presence of low glucose (LG; L; 1.67 mM glucose/KRBH; 4 h) or high glucose (HG; H; 16.7 mM glucose/KRBH; 4 h), and the amounts of secreted insulin were measured by ELISA. White bars indicate insulin secretion upon exposure to low glucose. Black bars indicate insulin secretion upon exposure to high glucose. **(C)** MIN6 (*Ire1α*$^{fl/fl}$) cells were transiently transfected with WT PDI/PDIA1 or WT five PDIs. The expression of insulin was induced, and amounts of secreted insulin were measured as described in B. n = 3. **, P < 0.01. EV, empty vector.

Liu et al., 2005; Kadokura and Beckwith, 2009; Zito et al., 2010; Kadokura et al., 2013). We then detected and distinguished oxidized monomer proinsulin and mixed-disulfide complexes involving proinsulin and showed that IRE1α is required for the efficient folding of proinsulin in pancreatic β cells (Fig. 4, D and E; and Fig. S4, A and B).

What is the precise role of IRE1α in the promotion of proinsulin folding? We found that the expression levels of five PDI family proteins, PDI, PDIR, P5, ERp44, and ERp46, were significantly decreased in MIN6 (*Ire1α*$^{\Delta R/\Delta R}$) cells (Fig. 5, A and B; and Fig. S4 D) and in pancreatic islets of IRE1α$^{B(-/\Delta R)}$ mice (Fig. 5, C and D). In addition, the expression levels of the five PDIs were restored by reconstituting the IRE1α–XBP1 pathway in MIN6 (*Ire1α*$^{\Delta R/\Delta R}$) cells (Fig. 6, F and G). ChIP assays of the five candidate PDIs confirmed that XBP1s protein directly binds to the promoter regions of the five PDI family genes (Fig. 7). Thus, IRE1α is required for the increased expression of PDI, P5, PDIR, ERp44, and ERp46 in pancreatic β cells. Furthermore, proinsulin and insulin contents were also fully restored by reconstituting the IRE1α–XBP1 pathway in MIN6 (*Ire1α*$^{\Delta R/\Delta R}$) cells (Fig. 6, A, C, and D) because the decrease in proinsulin folding was associated with decreases in the expression of the five PDIs, which are downstream targets of the IRE1α–XBP1 pathway. In addition, PDI, P5, ERp44, and ERp46 formed mixed-disulfide complexes with newly synthesized proinsulin (Fig. 8 A). We therefore propose that IRE1α functions as a key regulator of oxidative folding of enzymes involved in proinsulin folding (Fig. 9).

Insulin is a representative secretory protein folded by disulfide bond formation in the ER, but it is not fully understood how proinsulin is folded in the ER. Recently, it was reported that the deletion of ERO1β, an ER disulfide oxidase that is highly expressed in pancreatic β cells, causes a decrease in insulin secretion and oxidative folding of proinsulin in mice (Zito et al., 2010). ERO1 maintains PDIs in their active oxidized forms. However, the PDIs involved in proinsulin folding are not well characterized. In this study, we clearly showed that at least PDI, P5, ERp44, ERp46, and ERp72 form mixed-disulfide complexes with newly synthesized proinsulin (Fig. 8 A). In addition, decreased

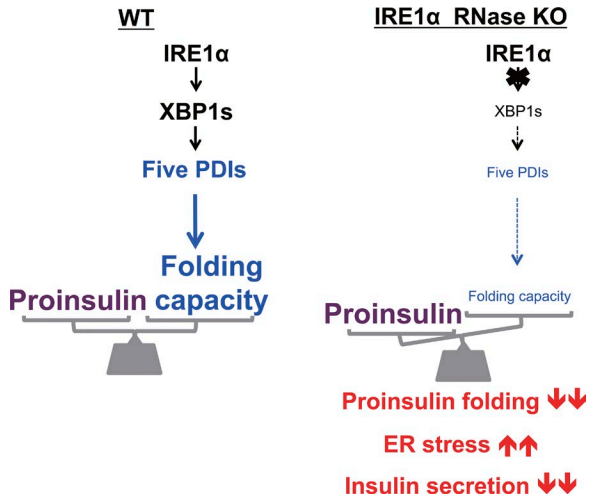

Figure 9. **Schematic diagram illustrating the function of IRE1α as a key regulator of oxidative proinsulin folding and PDI family levels in pancreatic β cells.**

expression of the five PDIs (PDI, P5, PDIR, ERp44, and ERp46) is correlated with decreased proinsulin folding (Figs. 4, 5, and 6), and reconstitution of the five PDIs could moderately restore insulin secretion to a similar extent as reconstitution of *Ire1α* (Figs. 6 E and 8 B). Furthermore, when we overexpressed the mixture of five PDIs in MIN6 ($Ire1\alpha^{fl/fl}$) cells, insulin secretion was increased. In contrast, the only PDI/PDIA1 overexpression in MIN6 ($Ire1\alpha^{fl/fl}$) cells had an inhibitory effect on insulin secretion (Fig. 8 C). Inhibitory effects of PDI/PDIA1 overexpression have been reported by other groups (Zhang et al., 2009; Rajpal et al., 2012). These findings also support our idea that the combination of five PDIs (PDI, P5, PDIR, ERp44, and ERp46) is required for correct proinsulin folding in the ER, leading to increased insulin secretion in response to high-glucose conditions in pancreatic β cells. However, further studies are required to elucidate their precise roles in this process.

Recently, two independent groups reported that the IRE1α–XBP1 pathway is required for insulin production and secretion in pancreatic β cells (Lee et al., 2011; Hassler et al., 2015). The main phenotypes of CKO mice are similar to those observed in this study. However, the proposed models explaining the phenotypes differ. Lee et al. (2011) reported that deletion of *Xbp1* in pancreatic β cells in mice decreased the mRNA expression of genes encoding Ins proteins, insulin-processing enzymes, and regulators of insulin secretion via the cleavage and degradation of their mRNAs by the RNase activity of IRE1α. Because the *Ire1α* CKO mice described by Hassler et al. (2015) and our group did not show such phenotypes, there were some differences between *Ire1α* CKO mice and *Xbp1* CKO mice. Hassler et al. (2015) reported that deletion of *Ire1α* in pancreatic β cells of mice caused decreased targeting of preproinsulin into the ER and decreased exocytosis of insulin. They showed decreased targeting of preproinsulin to the ER by transfection of the *Ins* gene with dominant-negative *IRE1α* or *XBP1s* into COS7 cells (Hassler et al., 2015). In this study, we used MIN6 ($Ire1\alpha^{\Delta R/\Delta R}$) cells to analyze preproinsulin targeting to the ER, and we did not detect such a difference. Thus, the differences among studies may be explained primarily by the differences among cell lines.

In this study, we used two independent experimental models, $IRE1\alpha^{B(-/\Delta R)}$ mice and MIN6 ($Ire1\alpha^{\Delta R/\Delta R}$) cells, and showed that constitutively activated IRE1α in pancreatic β cells induces specific PDI family proteins that are important for the correct folding of proinsulin in the ER. This combination technique is useful to clarify the novel roles of IRE1α in pancreatic β cells.

Materials and methods

Generation of $IRE1\alpha^{B(-/\Delta R)}$ mice

The $Ire1\alpha^{+/-}$ (deleted transmembrane domain) and $Ire1\alpha^{fl/fl}$ mice (floxed RNase domain) were generated as previously described (Iwawaki et al., 2009). To generate $Ire1\alpha^{-/fl}$ mice, $Ire1\alpha^{fl/fl}$ mice were crossed with $Ire1\alpha^{+/-}$ mice. $IRE1\alpha^{B(-/\Delta R)}$ mice were made by crossing these mice with the Ins-Cre transgenic mice Tg(Ins2-cre)23Herr, which were a generous gift from P. Herrera via Y. Kido (Kobe University, Kobe, Japan; Herrera, 2000). All experimental protocols involving animals were approved by the Committee on Animal Research at Nara Institute of Science and Technology (NAIST) and were performed in accordance with the institutional guidelines of NAIST.

Measurement of blood glucose and serum insulin

The blood glucose level was measured using LabAssay glucose (Wako). The insulin concentration in serum was determined using a mouse insulin ELISA kit (AKRIN-011T; Shibayagi).

Glucose tolerance tests

Glucose tolerance tests were performed on 12-wk-old male $IRE1\alpha^{B(\Delta R/-)}$ mice and $IRE1\alpha^{B(\Delta R/+)}$ mice after fasting for 16 h. Mice were administered glucose at 2 g/kg body weight by i.p. injection. Blood glucose levels were measured at 0, 15, 30, 60, and 120 min after the injection.

Islet morphology analysis and immunohistochemistry

The pancreas was fixed in 4% paraformaldehyde in PBS buffer at 4°C overnight and then immersed in 30% sucrose in PBS buffer. The pancreas was embedded in optimal cutting temperature compound. Immunohistochemistry was performed on 8-µm tissue sections prepared using a cryostat (HM550; MICROM International) following standard methods. Primary antibodies were used at the following dilutions: guinea pig antiinsulin (Dako) at a 1:500 dilution and rabbit antiglucagon (Dako) at a 1:500 dilution. Images of stained sections were observed using a fluorescence microscope (BZ-X710; Keyence) with a CFI Plan Apochromat Fluor 20× 0.5 NA objective lens (Nikon) at room temperature. The acquired images were processed with Imaging Joint BZ-H3XD and analyzed by BZ-H3A and BZ-H3C software (Keyence).

Islet isolation

Pancreatic islets were prepared from the mouse pancreas. HBSS (0.8% NaCl, 5 mM KCl, 0.17 mM Na_2HPO_4, 0.4 mM KH_2PO_4, 0.1% glucose, 1.2 mM $CaCl_2$, 0.8 mM $MgSO_4$, 7.5 mM $NaHCO_3$, and 0.01% phenol red) was used for perfusion and washing of the pancreas. Collagenase P (Roche) was dissolved in HBSS to a final

concentration of 1.5 mg/ml. The pancreas was perfused from the bile duct using 3 ml of the collagenase solution and was incubated at 37°C for 20 min. The collagenase was washed out with ice-cold HBSS with 10% newborn calf serum (16010; Gibco), and then islets were isolated from the collagenase-treated pancreas using the histopaque-1077 (Sigma-Aldrich) gradients. In brief, collagenase-treated tissues were gently resuspended in 10 ml ice-cold histopaque, and this solution was poured into 50-ml conical tubes. The ice-cold HBSS (10 ml) without newborn calf serum was slowly layered on the histopaque solution–containing islets. The tube was centrifuged at 1,700 *g* at 4°C for 20 min, the fraction of islets located in the boundary layer was collected and washed twice with 20 ml of ice-cold HBSS, and then islets were picked with a P-20 pipette (Gilson) into the Petri dish containing ice-cold HBSS using a dissecting microscope.

Establishment of mouse insulinoma cells harboring the floxed *Ire1α*-RNase domain

Ire1α$^{fl/fl}$ mice (Iwawaki et al., 2009) were crossed with IT-6 mice (Miyazaki et al., 1990, 2010), which express SV40 large T antigen under the control of the human insulin promoter. Progeny with the IT-6 transgene and homozygous floxed *Ire1α* alleles were obtained (*Ire1α*$^{fl/fl}$; IT-6 mice), and these mice developed insulinomas at 10 wk of age. Four MIN6 (*Ire1α*$^{fl/fl}$) cell lines were established from insulinomas that developed in independent mice. One MIN6 (*Ire1α*$^{fl/fl}$) cell line (original name; MINS#12) with high insulin secretion in high-glucose and high-insulin content was then selected (Sato et al., 2017). In the adenovirus infection experiments, two experimental controls were used. In one control, referred to as Con, MIN6 (*Ire1α*$^{fl/fl}$) cells, the MIN6 (*Ire1α*$^{fl/fl}$) cells were subjected to the infection procedure in the absence of adenovirus. In the other control, named Ad-GFP, MIN6 (*Ire1α*$^{fl/fl}$) cells, the cells were infected with adenovirus carrying GFP (Fig. S2 B).

Propagation and purification of adenovirus for the infection of MIN6 (*Ire1α*$^{fl/fl}$) cells

Adenovirus harboring either GFP or Cre has been described previously (Miyazaki et al., 2012). To propagate adenoviruses, HEK293 cells were infected with the appropriate adenovirus and grown for 3–5 d. To concentrate the adenovirus, the infected HEK293 cells were collected in a 50-ml tube and subjected to seven freeze–thaw cycles. After centrifugation at 3,500 *g* at 4°C for 30 min, the supernatants were collected and filtered to purify the adenovirus. The titer of the adenovirus was determined by the infectious titer method using HEK293 cells. MIN6 (*Ire1α*$^{fl/fl}$) cells were infected with adenovirus containing GFP or Cre at an MOI of 25 and cultured in DMEM containing 15% FBS (35–010-CV; Corning) and 55 μM β-mercaptoethanol.

Establishment of a stable cell line that expresses IRE1α or XBP1s

To reconstitute the IRE1α–XBP1 pathway in MIN6 (*Ire1α*$^{\Delta R/\Delta R}$) cells, WT *Ire1α* or *Xbp1s* was ligated into the pMXsIP-based retroviral vector (a gift from T. Kitamura, University of Tokyo, Tokyo, Japan) to construct *Ire1α*_pMXsIP and *Xbp1s*_pMXsIP. Plat-GP (RV-103; Cell Biolabs) cells were transfected with VSV-G_pMLV.2 and *Ire1α*_pMXsIP or *Xbp1s*_pMXsIP using Fugene HD (Promega) following the manufacturer's protocol to generate the retrovirus. VSV-G expressed by VSV-G_pMLV.2 promotes the formation and release into the culture medium of the virus particle. MIN6 (*Ire1α*$^{\Delta R/\Delta R}$) cells were infected with retroviruses and cultured for 1 wk in the presence of 5 μg/ml puromycin (Wako) to obtain MIN6 (*Ire1α*$^{\Delta R/\Delta R}$) cells stably expressing WT *Ire1α* and *Xbp1s*.

Cell culture

MIN6 (*Ire1α*$^{fl/fl}$ or *Ire1α*$^{\Delta R/\Delta R}$) cells were grown in DMEM containing 15% FBS and 55 μM β-mercaptoethanol. HEK293 and Plat-GP cells were cultured in DMEM containing 10% FCS. All cell lines were maintained in a humidified incubator with 95% air and 5% CO_2 at 37°C.

Antibodies for immunostaining

Immunostaining was performed with the following antibodies: antiinsulin at a 1:500 dilution and antiglucagon at a 1:500 dilution. The following secondary antibodies were used for detection: anti–guinea pig IgG (H+L chain) pAb–Alexa Fluor 488 (706-545-148; Jackson ImmunoResearch Laboratories, Inc.) at a 1:500 dilution and anti–rabbit IgG (H+L chain) pAb–Alexa Fluor 594 (A-21207; Thermo Fisher Scientific) at a 1:500 dilution.

Antibodies for immunoblotting

The following primary antibodies were used for immunoblotting: antiinsulin (8138S; Cell Signaling Technology) at a 1:1,000 dilution, anti-IRE1α (3294S; Cell Signaling Technology) at a 1:500 dilution, anti-PERK (3192S; Cell Signaling Technology) at a 1:500 dilution, anti–PERK-P (3179S; Cell Signaling Technology) at a 1:500 dilution, anti-eIF2α (5324S; Cell Signaling Technology) at a 1:1,000 dilution, anti–eIF2α-P (3398S; Cell Signaling Technology) at a 1:1,000 dilution, anti-GAPDH (5174S; Cell Signaling Technology) at a 1:1,000 dilution, anti-PDI (Kadokura et al., 2013) at a 1:1,000 dilution, anti-P5 (GTX121275; GeneTex) at a 1:1,000 dilution, anti-PDIR (sc-390862; Santa Cruz Biotechnology, Inc.) at a 1:200 dilution, anti-ERp44 (3798S; Cell Signaling Technology) at a 1:2,000 dilution, anti-ERp46 (a gift from K. Inaba, Tohoku University, Sendai, Japan) at a 1:2,000 dilution, anti-ERp72 (ab155800; Abcam) at a 1:1,000 dilution, anti-KDEL (ADI-SPA-827-J; Enzo Life Sciences) at a 1:500 dilution, anti-ORP150 (a gift from L. Hendershot, St. Jude Children's Research Hospital, Memphis, TN) at a 1:1,000 dilution, and anti-ATF6α and anti-ATF6β (Iwawaki et al., 2009) at a 1:2,000 dilution. The following secondary antibodies were used for immunoblotting: anti-IgG (H+L chain; rabbit) pAb-HRP goat IgG/Fab (458; MBL) at a 1:2,500 dilution and anti–mouse IgG-HRP (115-035-003; Jackson ImmunoResearch Laboratories, Inc.) at a 1:2,500 dilution.

Immunoblotting

MIN6 (*Ire1α*$^{fl/fl}$ or *Ire1α*$^{\Delta R/\Delta R}$) or MIN6 cells were plated on six-well plates at 4.0 × 10^6 cells/well, cultured for 4 d, and washed twice with PBS. They were subjected to alkylation with NEM and immunoblotting as previously described (Kadokura et al., 2013).

Coimmunoprecipitation experiment

WT MIN6 cells were transfected with FLAG-tagged PDI, PDIR, P5, ERp44, ERp46, ERp57, ERp72, and ERdj5 (a gift from K. Nagata,

Kyoto Sangyo University, Kyoto, Japan; Araki et al., 2013) and subjected to a pulse-chase experiment. Then, samples were subjected to alkylation with NEM and immunoprecipitation with an anti-FLAG monoclonal M2 antibody (F1804-5MG; Sigma-Aldrich). The resulting immunoprecipitates were then subjected to a second immunoprecipitation using antiproinsulin monoclonal antibody and separated by 4–12% NuPAGE (WG1402A; Thermo Fisher Scientific).

Quantification of secreted insulin by ELISA

MIN6 (*Ire1α*$^{fl/fl}$ or *Ire1α*$^{\Delta R/\Delta R}$) cells were plated on six-well plates at 4.0 × 10^6 cells/well, cultured for 4 d with DMEM, and preincubated for 2 h with Hepes–Krebs-Ringer bicarbonate Hepes (KRBH) buffer (10 mM Hepes, 115 mM NaCl, 5.9 mM KCl, 1.2 mM $MgCl_2$ $6H_2O$, 1.2 mM NaH_2PO_4, 1.2 mM Na_2SO_4, 2.5 mM $CaCl_2$, 25 mM $NaHCO_3$, and 2 mg/ml BSA) containing 1.67 mM glucose. MIN6 cells were then grown for 4 h under 1.67 mM glucose/Hepes-KRBH or 16.7 mM glucose/Hepes-KRBH. Insulin secreted into the culture medium was quantified by sandwich ELISA. The amount of secreted insulin was normalized against the total cellular protein.

Genotyping PCR

For genotyping PCR, tails of mice or MIN6 (*Ire1α*$^{fl/fl}$ or *Ire1α*$^{\Delta R/\Delta R}$) cells were collected in tubes and dissolved in tail lysis buffer (50 mM Tris-HCl, pH 7.5, 20 mM EDTA, pH 8.0, 100 mM NaCl, and 1% SDS) containing proteinase K (1:100; Takara Bio Inc.) at 65°C overnight. The dissolved samples were subjected to PCR amplification with primers (see below) and Ex-Taq DNA polymerase (Takara Bio Inc.). Mice and MIN6 (*Ire1α*$^{fl/fl}$ or *Ire1α*$^{\Delta R/\Delta R}$) cells were genotyped by PCR with primers that flank the loxP site (floxed) of the RNase domain of IRE1α, a transmembrane region of IRE1α, and rat insulin promoter-Cre region (see below). CreFlpCheck forward, 5′-CCGAGCCATGAGAAACAAGG-3′; CreFlpCheck reverse, 5′-CCCTGCCAGGATGGTCATGG-3′; 3Rcheck forward, 5′-CAAGTGAGGCGTATGACCTTCTG-3′; IRE1α-ex16-F1, 5′-GCTTCATCAGACCACCTCAG-3′; pgk-neo-R1, 5′-CGGTGGATG TGGAATGTGTG-3′; IRE1α-int17-R1, 5′-AGGGTCTGTCCTTAGAGA AC-3′; Cre-F001, 5′-ATGTCCAATTTACTGACCG-3′; and Cre-R001, 5′-CGCCGCATAACCAGTGAAAC-3′. The PCR products were separated on a 4% (floxed and transmembrane region of IRE1α) or 0.8% (Ins-Cre) agarose gel in tris, acetic acid, and EDTA (TAE) buffer and visualized after staining with ethidium bromide.

Transmission electron microscopy

MIN6 (*Ire1α*$^{fl/fl}$ or *Ire1α*$^{\Delta R/\Delta R}$) cells were seeded onto Thermanox plastic coverslips (Thermo Fisher Scientific). Cells were fixed in 0.1 M sodium cacodylate buffer, pH 7.4, containing 2.5% glutaraldehyde overnight at 4°C, and subsequently fixed in 0.1 M sodium cacodylate buffer, pH 7.4, containing 1% osmium tetroxide for 1 h at 4°C. Fixed cells were stained en bloc with 0.5% uranium acetate for 1 h at 4°C. The cells were dehydrated with a series of increasing ethanol concentrations and embedded in Epon812 (TAAB; Berks). Then, ultrathin sections (~90 nm) were cut with Ultracut UCT (Leica Microsystems), stained with aqueous lead citrate and uranyl acetate, and examined with an H7100 transmission electron microscope (Hitachi) at an acceleration voltage of 75 kV.

RNA extraction

Total RNA was isolated from mouse tissues and MIN6 cells using RNAiso PLUS (Takara Bio Inc.). cDNA was generated from total RNA using OligodT 18mer and Moloney murine leukemia virus reverse transcriptase (M-MLV; Promega) following the manufacturer's protocol.

Estimation of the extent of *Xbp1* mRNA splicing using RT-PCR

To estimate the extent of *Xbp1* mRNA splicing, cDNA prepared from total RNA as described above was subjected to PCR amplification with a pair of primers, i.e., mouse *Xbp1* forward primer, 5′-GAGAACCAGGAGTTAAGAACACG-3′; and mouse *Xbp1* reverse primer, 5′-GAAGATGTTCTGGGGAGGTGAC-3′; and KAPA Taq extra DNA polymerase (KAPA Bioscience). To evaluate the spliced and unspliced forms of *Xbp1u* mRNA, the PCR products were separated on a 7.5% acrylamide gel with TAE buffer and visualized after staining with ethidium bromide. Intensities of bands were then measured and used to determine the extent of *Xbp1* splicing.

qRT-PCR

To estimate the RNA expression of genes, cDNA prepared from total RNA as described above was subjected to qRT-PCR using SYBR green II (Takara Bio Inc.) with a pair of primers (Table S1) on a Light Cycler 480 system (Roche). Primers for RT-PCR were designed using Probe Finder (Roche).

ChIP assay

MIN6 cells were plated on 15-cm dishes and cultured for 4 d and then fixed in 1% paraformaldehyde/PBS for 10 min at room temperature. Chromatin shearing and immunoprecipitation were performed using the ChIP-IT Express chIP kit (53008; Active Motif) and Bioruptor UCW-310 (Sonic Bio) according to the manufacture's protocol. The immunoprecipitated DNA fragments were used as templates for PCR amplification (see below; the number +1 indicates the transcription start site of each gene). *Bip*-ChIP forward, 5′-ATGCTGCCTCTCATTGGTGGCCGTTAAG-3′ (approximately −198 through −226); *Bip*-ChIP reverse, 5′-TCA GTGTTGTCTCGGCCAGTATCGAG-3′ (approximately −1 through −25); *Pdi*-ChIP forward, 5′-TACGGAAACGCGGTCCAGTCAGAA TGC-3′ (approximately −437 through −464); *Pdi*-ChIP reverse, 5′-TGATTGGTGGAGAGATGCGCGTACC-3′ (approximately −324 through −349); *Pdir*-ChIP forward, 5′-TGGTTCTGATTCTGCGGG CACAGAGC-3′ (approximately −201 through −227); *Pdir*-ChIP reverse, 5′-AACAGCTACGGCCACTTCACAGCC-3′ (approximately +23 through +47); *P5*-ChIP forward, 5′-TTGGCCACGCACATG AGCGAAGTCC-3′ (approximately −111 through −136); *P5*-ChIP reverse, 5′-ATGCCGATCACCCGCATTCTGTCC-3′ (approximately +16 through +40); *Erp44*-ChIP forward, 5′-AAAGAGAGTCCCAGC TCTCCGATGAC-3′ (approximately −85 through −111); *Erp44*-ChIP reverse, 5′-AGGAGCAGCAAGGAGCATCTGAGGTC-3′ (approximately +179 through +205); *Erp46*-ChIP forward, 5′-ACACCA AGAGACCCGAGAGT-3′ (Lampropoulou et al., 2016); and *Erp46*-ChIP reverse, 5′-GTGGTTTCATCACACCCCCT-3′ (Lampropoulou et al., 2016). The PCR products were separated on a 3% agarose gel in TAE buffer and visualized after staining with ethidium bromide. Fold enrichment was quantified by TB green premix

Ex-Taq guanine-cytosine buffer (Perfect Real Time; Takara Bio Inc.) according to the manufacturer's protocol.

Antibodies for chIP assay

The following antibodies were used for chIP assays: normal rabbit IgG (2729; Cell Signaling Technology) at a 1:200 dilution and anti-XBP1s (619502; BioLegend) at a 1:100 dilution.

Pulse-chase, alkylation, and immunoprecipitation

MIN6 (*Ire1α*$^{fl/fl}$ or *Ire1α*$^{\Delta R/\Delta R}$) or WT MIN6 cells were pulse-labeled with 30 µl of EasyTag express [^{35}S] protein labeling mix (NEG772; PerkinElmer) in 16.7 mM glucose/Hepes-KRBH for the indicated times and were then chased by growing the cells in 16.7 mM glucose/Hepes-KRBH containing 0.13 mg/liter cysteine $2H_2O$ and 0.06 mg/ml methionine for the total duration. After these steps, free cysteines in the cells were subjected to alkylation with NEM as described above. The NEM-treated samples were then diluted ten-fold with ice-cold radioimmunoprecipitation assay buffer without SDS (150 mM NaCl, 1% NP-40, 0.5% deoxycholate, and 50 mM Tris-HCl, pH 8.0) and incubated with an antiproinsulin monoclonal antibody at 4°C for 16 h. The immune complexes were collected using Dynabeads protein G (10003D; Thermo Fisher Scientific). The eluted immune complexes were separated by 4–12% NuPAGE gel (WG1402A; Thermo Fisher Scientific), and the gel was exposed to an imaging plate for 2–10 d. The radioactive bands were detected using a BAS1000 system (Fujix).

Statistical analyses

Statistical significance was calculated by unpaired two-tailed Student's *t* test unless otherwise indicated. All experiments were repeated at least three times unless otherwise described. The number of independent experiments is described as *n*, and p-values (*, $P < 0.05$; **, $P < 0.01$) are indicated in the figure legends. Error bars in the figures represent SD. Data distribution was assumed to be normal, but this was not formally tested.

Online supplemental material

Fig. S1 shows the immunostaining of pancreas sections of IRE1α$^{B(+/\Delta R)}$ and IRE1α$^{B(-/\Delta R)}$ mice. Fig. S2 shows the scheme of mouse mating for the establishment of MIN6 cells with a floxed RNase domain of *Ire1α*. Fig. S3 shows that PERK and ATF6α pathways were activated in IRE1α RNase domain–KO MIN6 cells. Fig. S4 shows the detection of oxidative folding of proinsulin as well as RNA expression levels of ER chaperones and PDI family proteins. Table S1 shows the real-time PCR primer sequences.

Acknowledgments

We thank Fumiko Arai and Yusaku Nakamura for contributions to preliminary experimental data, Hitomi Ichikawa for electron microscopy, and Naoko Fujimoto, Junko Iida, Masami Yoshida, Azumi Wada, and Kazumi Maekawa for technical support. We thank Linda Hendershot for the ORP150 antibody, Kenji Inaba for the ERp46 antibody, Kazuhiro Nagata for the PDI family constructs, Toshio Kitamura for retrovirus vectors, and Pedro Herrera for Ins-Cre mice.

This work was supported in part by Japan Society for the Promotion of Science KAKENHI grants JP24228002, JP26116006, and JP17H01468 (to K. Kohno), a Ministry of Education, Culture, Sports, Science and Technology KAKENHI grant JP19058010 (to K. Kohno), Takeda Science Foundation (to K. Kohno), Japan Society for the Promotion of Science KAKENHI grant JP26430090 (to M. Saito), Japan Society for the Promotion of Science KAKENHI grants JP15K07381 and JP26116005 (to H. Kadokura), and Noda Institute for Scientific Research (to H. Kadokura).

The authors declare no competing financial interests.

Author contributions: Y. Tsuchiya established MIN6 (*Ire1α*$^{fl/fl}$) cell lines and performed all experiments using cultured cells. M. Saito generated mouse strains and performed all experiments related to the mouse studies. J.-i. Miyazaki and F. Tashiro provided IT-6 mice and prepared adenovirus. T. Iwawaki provided IRE1α KO, CKO mice, and anti-ATF6 antibody. H. Kadokura designed the analysis of oxidative proinsulin folding. Y. Imagawa performed electron micrograph analyses. Y. Tsuchiya, M. Saito, H. Kadokura, and K. Kohno conceived the research, analyzed the data, and wrote the manuscript. K. Kohno supervised all studies. All authors discussed the results and commented on the manuscript.

Submitted: 26 July 2017
Revised: 6 December 2017
Accepted: 22 January 2018

References

Acosta-Alvear, D., Y. Zhou, A. Blais, M. Tsikitis, N.H. Lents, C. Arias, C.J. Lennon, Y. Kluger, and B.D. Dynlacht. 2007. XBP1 controls diverse cell type- and condition-specific transcriptional regulatory networks. *Mol. Cell.* 27:53–66. https://doi.org/10.1016/j.molcel.2007.06.011

Araki, K., S. Iemura, Y. Kamiya, D. Ron, K. Kato, T. Natsume, and K. Nagata. 2013. Ero1-α and PDIs constitute a hierarchical electron transfer network of endoplasmic reticulum oxidoreductases. *J. Cell Biol.* 202:861–874. https://doi.org/10.1083/jcb.201303027

Arensdorf, A.M., D. Diedrichs, and D.T. Rutkowski. 2013. Regulation of the transcriptome by ER stress: non-canonical mechanisms and physiological consequences. *Front. Genet.* 4:256. https://doi.org/10.3389/fgene.2013.00256

Bertolotti, A., X. Wang, I. Novoa, R. Jungreis, K. Schlessinger, J.H. Cho, A.B. West, and D. Ron. 2001. Increased sensitivity to dextran sodium sulfate colitis in IRE1beta-deficient mice. *J. Clin. Invest.* 107:585–593. https://doi.org/10.1172/JCI11476

Braakman, I., and N.J. Bulleid. 2011. Protein folding and modification in the mammalian endoplasmic reticulum. *Annu. Rev. Biochem.* 80:71–99. https://doi.org/10.1146/annurev-biochem-062209-093836

Calfon, M., H. Zeng, F. Urano, J.H. Till, S.R. Hubbard, H.P. Harding, S.G. Clark, and D. Ron. 2002. IRE1 couples endoplasmic reticulum load to secretory capacity by processing the XBP-1 mRNA. *Nature.* 415:92–96. https://doi.org/10.1038/415092a

Engin, F., A. Yermalovich, T. Nguyen, S. Hummasti, W. Fu, D.L. Eizirik, D. Mathis, and G.S. Hotamisligil. 2013. Restoration of the unfolded protein response in pancreatic β cells protects mice against type 1 diabetes. *Sci. Transl. Med.* 5:211ra156. https://doi.org/10.1126/scitranslmed.3006534

Engin, F., T. Nguyen, A. Yermalovich, and G.S. Hotamisligil. 2014. Aberrant islet unfolded protein response in type 2 diabetes. *Sci. Rep.* 4:4054. https://doi.org/10.1038/srep04054

Han, D., A.G. Lerner, L. Vande Walle, J.P. Upton, W. Xu, A. Hagen, B.J. Backes, S.A. Oakes, and F.R. Papa. 2009. IRE1alpha kinase activation modes control alternate endoribonuclease outputs to determine divergent cell fates. *Cell.* 138:562–575. https://doi.org/10.1016/j.cell.2009.07.017

Han, S.I., K. Yasuda, and K. Kataoka. 2011. ATF2 interacts with beta-cell-enriched transcription factors, MafA, Pdx1, and beta2, and activates insulin gene transcription. *J. Biol. Chem.* 286:10449–10456. https://doi.org/10.1074/jbc.M110.209510

Harding, H.P., H. Zeng, Y. Zhang, R. Jungries, P. Chung, H. Plesken, D.D. Sabatini, and D. Ron. 2001. Diabetes mellitus and exocrine pancreatic dysfunction in perk-/- mice reveals a role for translational control in secretory cell survival. *Mol. Cell.* 7:1153–1163. https://doi.org/10.1016/S1097-2765(01)00264-7

Harding, H.P., A.F. Zyryanova, and D. Ron. 2012. Uncoupling proteostasis and development in vitro with a small molecule inhibitor of the pancreatic endoplasmic reticulum kinase, PERK. *J. Biol. Chem.* 287:44338–44344. https://doi.org/10.1074/jbc.M112.428987

Hassler, J.R., D.L. Scheuner, S. Wang, J. Han, V.K. Kodali, P. Li, J. Nguyen, J.S. George, C. Davis, S.P. Wu, et al. 2015. The IRE1α/XBP1s Pathway Is Essential for the Glucose Response and Protection of β Cells. *PLoS Biol.* 13:e1002277. https://doi.org/10.1371/journal.pbio.1002277

Herrera, P.L. 2000. Adult insulin- and glucagon-producing cells differentiate from two independent cell lineages. *Development.* 127:2317–2322 http://dev.biologists.org/content/127/11/2317.long.

Iwawaki, T., R. Akai, K. Kohno, and M. Miura. 2004. A transgenic mouse model for monitoring endoplasmic reticulum stress. *Nat. Med.* 10:98–102. https://doi.org/10.1038/nm970

Iwawaki, T., R. Akai, S. Yamanaka, and K. Kohno. 2009. Function of IRE1 alpha in the placenta is essential for placental development and embryonic viability. *Proc. Natl. Acad. Sci. USA.* 106:16657–16662. https://doi.org/10.1073/pnas.0903775106

Iwawaki, T., R. Akai, and K. Kohno. 2010. IRE1α disruption causes histological abnormality of exocrine tissues, increase of blood glucose level, and decrease of serum immunoglobulin level. *PLoS One.* 5:e13052. https://doi.org/10.1371/journal.pone.0013052

Kadokura, H., and J. Beckwith. 2009. Detecting folding intermediates of a protein as it passes through the bacterial translocation channel. *Cell.* 138:1164–1173. https://doi.org/10.1016/j.cell.2009.07.030

Kadokura, H., M. Saito, A. Tsuru, A. Hosoda, T. Iwawaki, K. Inaba, and K. Kohno. 2013. Identification of the redox partners of ERdj5/JPDI, a PDI family member, from an animal tissue. *Biochem. Biophys. Res. Commun.* 440:245–250. https://doi.org/10.1016/j.bbrc.2013.09.063

Kimata, Y., and K. Kohno. 2011. Endoplasmic reticulum stress-sensing mechanisms in yeast and mammalian cells. *Curr. Opin. Cell Biol.* 23:135–142. https://doi.org/10.1016/j.ceb.2010.10.008

Kimata, Y., Y. Ishiwata-Kimata, T. Ito, A. Hirata, T. Suzuki, D. Oikawa, M. Takeuchi, and K. Kohno. 2007. Two regulatory steps of ER-stress sensor Ire1 involving its cluster formation and interaction with unfolded proteins. *J. Cell Biol.* 179:75–86. https://doi.org/10.1083/jcb.200704166

Lampropoulou, E., A. Lymperopoulou, and A. Charonis. 2016. Reduced expression of ERp46 under diabetic conditions in β-cells and the effect of liraglutide. *Metabolism.* 65:7–15. https://doi.org/10.1016/j.metabol.2015.09.011

Lee, A.H., G.C. Chu, N.N. Iwakoshi, and L.H. Glimcher. 2005. XBP-1 is required for biogenesis of cellular secretory machinery of exocrine glands. *EMBO J.* 24:4368–4380. https://doi.org/10.1038/sj.emboj.7600903

Lee, A.H., K. Heidtman, G.S. Hotamisligil, and L.H. Glimcher. 2011. Dual and opposing roles of the unfolded protein response regulated by IRE1α and XBP1 in proinsulin processing and insulin secretion. *Proc. Natl. Acad. Sci. USA.* 108:8885–8890. https://doi.org/10.1073/pnas.1105564108

Li, H., A.V. Korennykh, S.L. Behrman, and P. Walter. 2010. Mammalian endoplasmic reticulum stress sensor IRE1 signals by dynamic clustering. *Proc. Natl. Acad. Sci. USA.* 107:16113–16118. https://doi.org/10.1073/pnas.1010580107

Lipson, K.L., S.G. Fonseca, S. Ishigaki, L.X. Nguyen, E. Foss, R. Bortell, A.A. Rossini, and F. Urano. 2006. Regulation of insulin biosynthesis in pancreatic beta cells by an endoplasmic reticulum-resident protein kinase IRE1. *Cell Metab.* 4:245–254. https://doi.org/10.1016/j.cmet.2006.07.007

Liu, M., Y. Li, D. Cavener, and P. Arvan. 2005. Proinsulin disulfide maturation and misfolding in the endoplasmic reticulum. *J. Biol. Chem.* 280:13209–13212. https://doi.org/10.1074/jbc.C400475200

Miyazaki, J., K. Araki, E. Yamato, H. Ikegami, T. Asano, Y. Shibasaki, Y. Oka, and K. Yamamura. 1990. Establishment of a pancreatic beta cell line that retains glucose-inducible insulin secretion: special reference to expression of glucose transporter isoforms. *Endocrinology.* 127:126–132. https://doi.org/10.1210/endo-127-1-126

Miyazaki, S., H. Taniguchi, Y. Moritoh, F. Tashiro, T. Yamamoto, E. Yamato, H. Ikegami, K. Ozato, and J. Miyazaki. 2010. Nuclear hormone retinoid X receptor (RXR) negatively regulates the glucose-stimulated insulin secretion of pancreatic ß-cells. *Diabetes.* 59:2854–2861. https://doi.org/10.2337/db09-1897

Miyazaki, S., R. Minamida, T. Furuyama, F. Tashiro, E. Yamato, S. Inagaki, and J. Miyazaki. 2012. Analysis of Foxo1-regulated genes using Foxo1-deficient pancreatic β cells. *Genes Cells.* 17:758–767. https://doi.org/10.1111/j.1365-2443.2012.01625.x

Mori, K. 2009. Signalling pathways in the unfolded protein response: development from yeast to mammals. *J. Biochem.* 146:743–750. https://doi.org/10.1093/jb/mvp166

Okada, T., K. Haze, S. Nadanaka, H. Yoshida, N.G. Seidah, Y. Hirano, R. Sato, M. Negishi, and K. Mori. 2003. A serine protease inhibitor prevents endoplasmic reticulum stress-induced cleavage but not transport of the membrane-bound transcription factor ATF6. *J. Biol. Chem.* 278:31024–31032. https://doi.org/10.1074/jbc.M300923200

Okumura, M., H. Kadokura, and K. Inaba. 2015. Structures and functions of protein disulfide isomerase family members involved in proteostasis in the endoplasmic reticulum. *Free Radic. Biol. Med.* 83:314–322. https://doi.org/10.1016/j.freeradbiomed.2015.02.010

Pechhold, K., X. Zhu, V.S. Harrison, J. Lee, S. Chakrabarty, K. Koczwara, O. Gavrilova, and D.M. Harlan. 2009. Dynamic changes in pancreatic endocrine cell abundance, distribution, and function in antigen-induced and spontaneous autoimmune diabetes. *Diabetes.* 58:1175–1184. https://doi.org/10.2337/db08-0616

Rajpal, G., I. Schuiki, M. Liu, A. Volchuk, and P. Arvan. 2012. Action of protein disulfide isomerase on proinsulin exit from endoplasmic reticulum of pancreatic β-cells. *J. Biol. Chem.* 287:43–47. https://doi.org/10.1074/jbc.C111.279927

Ron, D., and P. Walter. 2007. Signal integration in the endoplasmic reticulum unfolded protein response. *Nat. Rev. Mol. Cell Biol.* 8:519–529. https://doi.org/10.1038/nrm2199

Rutkowski, D.T., and R.S. Hegde. 2010. Regulation of basal cellular physiology by the homeostatic unfolded protein response. *J. Cell Biol.* 189:783–794. https://doi.org/10.1083/jcb.201003138

Sato, H., Y. Shiba, Y. Tsuchiya, M. Saito, and K. Kohno. 2017. 4μ8C inhibits insulin secretion independent of IRE1α RNase activity. *Cell Struct. Funct.* 42:61–70. https://doi.org/10.1247/csf.17002

Sharma, R.B., A.C. O'Donnell, R.E. Stamateris, B. Ha, K.M. McCloskey, P.R. Reynolds, P. Arvan, and L.C. Alonso. 2015. Insulin demand regulates β cell number via the unfolded protein response. *J. Clin. Invest.* 125:3831–3846. https://doi.org/10.1172/JCI79264

Szabat, M., M.M. Page, E. Panzhinskiy, S. Skovsø, M. Mojibian, J. Fernandez-Tajes, J.E. Bruin, M.J. Bround, J.T. Lee, E.E. Xu, et al. 2016. Reduced Insulin Production Relieves Endoplasmic Reticulum Stress and Induces β Cell Proliferation. *Cell Metab.* 23:179–193. https://doi.org/10.1016/j.cmet.2015.10.016

Tabas, I., and D. Ron. 2011. Integrating the mechanisms of apoptosis induced by endoplasmic reticulum stress. *Nat. Cell Biol.* 13:184–190. https://doi.org/10.1038/ncb0311-184

Tsuru, A., N. Fujimoto, S. Takahashi, M. Saito, D. Nakamura, M. Iwano, T. Iwawaki, H. Kadokura, D. Ron, and K. Kohno. 2013. Negative feedback by IRE1β optimizes mucin production in goblet cells. *Proc. Natl. Acad. Sci. USA.* 110:2864–2869. https://doi.org/10.1073/pnas.1212484110

Wang, S., S. Park, V.K. Kodali, J. Han, T. Yip, Z. Chen, N.O. Davidson, and R.J. Kaufman. 2015. Identification of protein disulfide isomerase 1 as a key isomerase for disulfide bond formation in apolipoprotein B100. *Mol. Biol. Cell.* 26:594–604. https://doi.org/10.1091/mbc.E14-08-1274

Wang, X., M.C. Zielinski, R. Misawa, P. Wen, T.Y. Wang, C.Z. Wang, P. Witkowski, and M. Hara. 2013. Quantitative analysis of pancreatic polypeptide cell distribution in the human pancreas. *PLoS One.* 8:e55501. https://doi.org/10.1371/journal.pone.0055501

Wang, Z.V., T.D. Schraw, J.Y. Kim, T. Khan, M.W. Rajala, A. Follenzi, and P.E. Scherer. 2007. Secretion of the adipocyte-specific secretory protein adiponectin critically depends on thiol-mediated protein retention. *Mol. Cell. Biol.* 27:3716–3731. https://doi.org/10.1128/MCB.00931-06

Weiss, M.A. 2009. Proinsulin and the genetics of diabetes mellitus. *J. Biol. Chem.* 284:19159–19163. https://doi.org/10.1074/jbc.R109.009936

Yamamoto, K., T. Sato, T. Matsui, M. Sato, T. Okada, H. Yoshida, A. Harada, and K. Mori. 2007. Transcriptional induction of mammalian ER quality control proteins is mediated by single or combined action of ATF6alpha and XBP1. *Dev. Cell.* 13:365–376. https://doi.org/10.1016/j.devcel.2007.07.018

Yanagitani, K., Y. Kimata, H. Kadokura, and K. Kohno. 2011. Translational pausing ensures membrane targeting and cytoplasmic splicing of XBP1u mRNA. *Science.* 331:586–589. https://doi.org/10.1126/science.1197142

Yoshida, H., T. Matsui, A. Yamamoto, T. Okada, and K. Mori. 2001. XBP1 mRNA is induced by ATF6 and spliced by IRE1 in response to ER stress to produce a highly active transcription factor. *Cell.* 107:881–891. https://doi.org/10.1016/S0092-8674(01)00611-0

Yoshida, H., T. Matsui, N. Hosokawa, R.J. Kaufman, K. Nagata, and K. Mori. 2003. A time-dependent phase shift in the mammalian unfolded protein response. *Dev. Cell.* 4:265–271. https://doi.org/10.1016/S1534-5807(03)00022-4

Zhang, L., E. Lai, T. Teodoro, and A. Volchuk. 2009. GRP78, but not protein-disulfide isomerase, partially reverses hyperglycemia-induced inhibition of insulin synthesis and secretion in pancreatic β-Cells. *J. Biol. Chem.* 284:5289–5298. https://doi.org/10.1074/jbc.M805477200

Zito, E., K.T. Chin, J. Blais, H.P. Harding, and D. Ron. 2010. ERO1-beta, a pancreas-specific disulfide oxidase, promotes insulin biogenesis and glucose homeostasis. *J. Cell Biol.* 188:821–832. https://doi.org/10.1083/jcb.200911086